NASA TECHNICAL NOTE

NASA TN D-7048

NASA TN D-7048

EXPERIMENTAL AERODYNAMIC PERFORMANCE CHARACTERISTICS OF A ROTOR ENTRY VEHICLE CONFIGURATION

III – Supersonic

by Ronald C. Smith and Alan D. Levin

Ames Research Center
Moffett Field, Calif. 94035

NATIONAL AERONAUTICS AND SPACE ADMINISTRATION • WASHINGTON, D. C. • FEBRUARY 1971

1. Report No.	2. Government Accession No.	3. Recipient's Catalog No.
NASA TN D-7048		

4. Title and Subtitle	5. Report Date
EXPERIMENTAL AERODYNAMIC PERFORMANCE CHARACTERISTICS OF A ROTOR ENTRY VEHICLE CONFIGURATION III – SUPERSONIC	February 1971
	6. Performing Organization Code
7. Author(s)	8. Performing Organization Report No.
Ronald C. Smith and Alan D. Levin	A-3711
	10. Work Unit No.
9. Performing Organization Name and Address	124-07-11-11-00-21
NASA Ames Research Center Moffett Field, Calif., 94035	11. Contract or Grant No.
	13. Type of Report and Period Covered
12. Sponsoring Agency Name and Address	Technical Note
National Aeronautics and Space Administration Washington, D. C., 20546	14. Sponsoring Agency Code

15. Supplementary Notes

16. Abstract

Wind-tunnel tests were conducted to determine the aerodynamic performance characteristics of an unpowered rotor entry vehicle configuration at Mach numbers from 1.62 to 3.54. Two rotor blade configurations with double-wedge and modified-ellipse profiles were tested at vehicle angles of attack from 15° to 90°. Variable blade collective pitch was used to control rotor rotational speed.

Results of the tests indicate that the rotor speed is well behaved and manually controllable through blade pitch. The maximum L/D varied from 0.75 at Mach number 1.62 to 0.68 at Mach number 3.54. The rotor produced destabilizing pitching moments rendering the basic configuration unstable and out of trim in glide flight. Cyclic feathering was found to be inadequate for longitudinal trim but was satisfactory for roll trim. The addition of body-mounted pitch flaps provided the necessary trim and eliminated the instability over most of the speed range.

17. Key Words (Suggested by Author(s))	18. Distribution Statement
Entry Vehicles Rotor Performance Rotor Aerodynamics Supersonic Autorotating Rotor Characteristics	Unclassified – Unlimited

19. Security Classif. (of this report)	20. Security Classif. (of this page)	21. No. of Pages	22. Price*
Unclassified	Unclassified	53	$3.00

*For sale by the National Technical Information Service, Springfield, Virginia 22151

NOTATION

The body-axes, force and moment coefficients, and angles used are shown in figure 1.

b number of blades

c blade chord

C_D drag coefficient, $\frac{\text{drag}}{q_\infty S}$

C_L lift coefficient, $\frac{\text{lift}}{q_\infty S}$

C_l body axis rolling-moment coefficient, $\frac{\text{rolling moment}}{q_\infty Sd}$

C_m pitching-moment coefficient, $\frac{\text{pitching moment}}{q_\infty Sd}$

C_N normal-force coefficient, $\frac{\text{normal coefficient}}{q_\infty S}$

C_X axial-force coefficient, $\frac{\text{axial force}}{q_\infty S}$

C_Y side-force coefficient, $\frac{\text{side force}}{q_\infty S}$

d capsule diameter

$\frac{L}{D}$ lift-drag ratio

M_∞ free-stream Mach number

q_∞ free-stream dynamic pressure

R rotor-blade radius measured normal to the axis of rotation with the blades in the fully open ($\beta = 0°$) position

R_{LE} blade section leading-edge radius

S capsule reference area, $\frac{\pi d^2}{4}$

V_∞ free-stream velocity

$(\Omega R)_0$ tip speed for no cyclic feathering

$\frac{\Omega R}{V_\infty}$ dimensionless tip speed

α angle of attack, angle between relative wind and a plane normal to the shaft axis

β flapping angle

$\theta(\psi)$ blade pitch angle, $\theta_0 - \theta_1 \sin \psi + \theta_2 \cos \psi$

θ_0 collective pitch angle

θ_1 longitudinal cyclic pitch (sine feathering amplitude)

θ_2 lateral cyclic pitch (cosine feathering amplitude)

σ rotor solidity, $\frac{bc}{\pi R}$

ψ blade azimuth angle

Ω rotor angular velocity

EXPERIMENTAL AERODYNAMIC PERFORMANCE CHARACTERISTICS OF A ROTOR ENTRY VEHICLE CONFIGURATION

III - SUPERSONIC

Ronald C. Smith and Alan D. Levin

Ames Research Center

SUMMARY

Wind-tunnel tests have been conducted to determine the aerodynamic and operating characteristics of an unpowered rotor entry vehicle configuration at Mach numbers from 1.62 to 3.54 over the angle-of-attack range from 15° to 90°. Rotor speed was varied through manual control of blade collective pitch. The effectiveness of rotor cyclic pitch controls in providing control moments was also investigated. A 45-inch-diameter rotor using two different blade airfoil sections was tested in combination with a 15-inch-diameter capsule forebody. The blade sections were a double wedge and a modified ellipse each with a 20-percent thickness ratio. Tests were also conducted with a pointed cone-cylinder forebody in place of the capsule to evaluate the effects of body-rotor interference.

Results of the tests indicate that the rotor speed is well behaved and manually controllable through blade pitch. The maximum L/D varied from 0.75 at Mach number 1.62 to 0.68 at Mach number 3.54. The variation of collective blade pitch had little effect on the lift, drag, or pitching moment but did affect the rotor rolling moment. The rotor produced destabilizing pitching moments rendering the basic configurations unstable and out of trim in glide flight. The cyclic pitch controls were found to be ineffective for pitch trim but were adequate for trimming the rolling moment in glide attitudes. The addition of flaps to the body provided pitch trim and eliminated the instability over most of the speed range tested. Body flow field interference substantially reduced the lift and drag of the rotor in near-axial flight attitudes.

INTRODUCTION

As the recovery of instrumented and manned space capsules becomes more frequent, the need for a recovery system that can provide a safe landing almost anywhere and in adverse weather becomes more urgent. While parachutes, paragliders, and lifting bodies can perform certain missions, none of these recovery systems has the operational flexibility needed to perform a large variety of recovery missions.

One system that appears to possess the desired capabilities is the deployable autorotating rotor. Specifically, the rotor offers the capability of (1) zero speed touchdown; (2) touchdown at an unprepared landing site; and (3) aerodynamic force modulation without changes in the vehicle's

attitude. The idea of using a rotor for lift and retardation during recovery from orbit is not new and has been investigated and reported by various authors (see refs. 1-5).

The investigation reported herein is part of a program designed to determine the feasibility of using an autorotating rotor for lift and drag modulation from orbital speed to touchdown. An analytical study has been made to estimate the aerodynamic characteristics of a rotor entry vehicle (REV) configuration and to determine its performance as an entry vehicle. This work has been reported in reference 6. The entry performance study indicated that the REV could provide substantial range capability if the aerodynamic heating of the rotor blades would not severely restrict the flight envelope. In order to establish the limits on velocity and altitude imposed by blade heating, experiments were made on a small REV model in the Ames 1-foot shock tunnel to measure blade heating rates (ref. 7). The results agree favorably with heating estimates for near-axial flight (flight nearly parallel to rotor axis) and indicate that the rotor can be used for retardation during the entire entry. Blade-leading-edge heating rates measured in glide flight were not valid because of the small size of the model. Heating rates estimated for the leading edge indicate that the rotor can be utilized in glide flight (15° to 27° angle of attack) at speeds below about 16,000 feet per second (200,000 ft altitude) using a radiation-cooled blade with a ceramic coating capable of withstanding 3700° F. The study reported in reference 6 indicated that delaying glide flight until a speed of 16,000 feet per second is reached would reduce lateral range from 650 statute miles (glide flight from orbit) to about 500 statute miles.

Unfortunately, all work on rotor systems to date was either theoretical or limited to tests at near-axial attitudes for high forward speeds. Hence, very little was known about the aerodynamic and operating characteristics (rotational speed versus blade pitch) of rotors in high-speed glide flight.

The objectives of the experimental test program, of which this report is a part, are to provide experimental rotor operating (RPM vs blade pitch) and aerodynamic characteristics to substantiate the entry performance of a REV as well as to add substantially to the knowledge of high speed unpowered rotors. Accordingly, a wind tunnel model of an REV configuration was built and successfully tested at Mach numbers up to 3.5 at angles of attack from 15° to 90°.

Table 1 indicates the scope of the experimental effort to determine the aerodynamic characteristics of the body-rotor configuration. This report is the third of a three-part series covering the three speed regimes tested. Parts I and II cover, respectively, the subsonic and transonic speed regimes. Results of these tests are reported in references 8 and 9 respectively.

MODEL DESCRIPTION

The rotor entry vehicle model tested is a four-bladed rotor mounted on a capsule body. The mechanical design and fabrication was accomplished by the Kaman Aircraft Corporation according to general specifications provided by NASA ARC. Detailed drawings of the model are shown in figure 2. Photographs of the model mounted in the Ames 8- by 7- and 9- by 7-foot wind tunnels are shown in figure 3.

Rotor

The rotor blades have variable collective pitch and cyclic pitch and were allowed to flap about offset flapping hinges within predetermined limits; however, they do not have lead-lag freedom. A capability was provided by means of a conventional swashplate for remotely changing both the collective and cyclic pitch either indepentently or in combination. The total range of collective pitch travel is ±90°, but only a 40° range is available through the use of the remote control system. The blades could be attached at 15° increments, which allowed the entire collective pitch range to be tested. Both the lateral (cosine feathering) and longitudinal (sine feathering) cyclic pitch amplitudes had a range of ±10°. The design operating tip speed is 1100 ft/sec. A detailed description of the model, control system features and strength requirements can be found in reference 10.

Blades

Two different blade airfoil sections, a modified ellipse and a double wedge, were tested and are illustrated in figure 2(b). These blades have a length which gives a rotor diameter of 45 inches and a solidity of 20 percent. The maximum thickness to chord ratio is 20 percent. The rotor blades are untwisted and have a rectangular planform. The rotor blades were fabricated of fiberglass epoxy laminate with most of the fibers oriented in the spanwise (radial) direction, giving the blades an extremely high strength-to-weight ratio in the radial direction.

Forebodies

The capsule body is a typical blunt entry vehicle (see fig. 2(a)) consisting of a body of revolution about the rotor axis. The maximum diameter of the body is 15 inches, which gives a rotor-to-capsule diameter ratio of 3. The cone-cylinder forebody that was used in place of the capsule body to simulate rotor-alone characteristics is shown in figure 2(d).

Model Mounting Details

In order to cover the angle-of-attack range from 0° to 90°, three different model mounting arrangements were used. In all cases the balance centerline was coincident with the rotor axis as shown in figure 4. For the angle-of-attack range from 0° to 27° (fig. 4(a)), the model and balance were mounted on a 90° elbow attached to the model support sting. In the range from 33° to 60° (fig. 4(b)) the model and balance were mounted on a 30° bent adapter attached to the sting. In the range from 63° to 90° (fig. 4(c)) the model and balance were mounted in line with the sting. For the angle-of-attack range from 33° to 90° the wind tunnel support system necessitated mounting the model upside down. For this range of angles of attack the model lift was positive in the downward direction.

Flapping stop- For the angles of attack from 0° to 27° a flapping stop (fig. 2(a)) was mounted on the rotor hub to prevent large flapping excursions of the rotor blades when the tunnel was started and when conditions that cause flapping instability occurred during the testing. This stop held flapping to 20°. When the model was mounted in the 33° to 60° attitude, a flapping stop was also required to prevent the rotor blades from striking the model support sting. This stop allowed up to 45° of flapping freedom. For tests in the axial configuration the flapping stop was removed.

Blade cager (axial mounting only)- A blade caging arrangement (fig. 5) was provided to hold the blades in a stowed position along the support sting during the tunnel starting operation. The cager could be used only when the model was mounted in the axial ($\alpha = 90°$) configuration. After the data were taken, the rotor could be stopped and re-caged before the tunnel was shut down. The caging mechanism was equipped to provide remote opening and closing.

INSTRUMENTATION AND TEST PROCEDURE

Instrumentation

The model forces were measured by means of 1.75-inch 6-component internal strain-gage balance. Rotor RPM was obtained from two magnetic pickups mounted on the stationary swashplate inside the model. The magnetic pickups are energized by the passage of teeth on the rotating swashplate producing an a.c. output at the tooth-passing frequency. A gap left by the omission of one tooth produces a gap in the harmonic output of each of the magnetic pickups. These gaps in the outputs when viewed simultaneously on a dual-beam oscilloscope allowed determination of the direction of rotation.

Test Procedure

When the tunnel was started with the model in the axial configuration ($\alpha = 90°$), the blades were stowed along the sting and held by the blade cager. After test conditions were reached in the tunnel, the cager was opened to allow deployment of the rotor. Both collective pitch and cyclic pitch are used to initiate the deployment which simulated deployment during the recovery process. Before shutting the tunnel down, the rotor was restowed by setting the blade pitch at zero. Under these conditions the rotation stops and the flow forces the blades back along the sting. Finally, the blades are clamped in place by closing the cage. This procedure was utilized to minimize the possibility of damage to the rotor during the tunnel shutdown operations. At low and intermediate angles of attack, rotor rotation was initiated at a free-stream dynamic pressure of about 50 psf by use of the collective pitch control.

In the glide attitude ($\alpha = 15°$ to $27°$) it was found to be "unsafe" to operate the rotor at angles of attack less than 15° because of flapping instability. This instability occurs when there is insufficient centrifugal force to generate the required moment about the flapping hinge to balance the aerodynamic moment. The resulting flapping excursions can easily cause blade failure by repeated contact of the blade grip with the flapping stop.

The investigation was conducted by parametrically varying the blade pitch angle at fixed conditions of angle of attack and free-stream Mach number. During the test operations only collective pitch and either longitudinal (sine feathering amplitude) cyclic pitch or lateral (cosine feathering amplitude) cyclic pitch were varied. When cyclic pitch was varied, the collective pitch angle was held constant. Throughout the tests the model was maintained at zero sideslip angle. Rotor rotation was always clockwise when viewed from the top.

WIND TUNNELS, TEST CONDITIONS AND DATA ACCURACY

The tests were conducted in the Ames 8- by 7-foot and 9- by 7-foot supersonic wind tunnels which have a combined test Mach number range continuously variable from 1.55 to 3.55. These wind tunnels are of the variable density, continuous flow type and are described fully in reference 11.

For the test Mach number range the free-stream dynamic pressure and Reynolds number based on capsule diameter were as follows:

M_∞	q_∞, lb/ft^2	Reynolds number
1.62	147	1.0×10^6
3.54	109	1.1×10^6

The force and moment elements of the balance used for these tests were sized for testing at dynamic pressures up to 500 psf. The dynamic pressures of the present tests produced loads no greater than one-fourth of balance capacity. The maximum uncertainties in the data are estimated as follows:

C_l	±0.02	M_∞	±0.01
C_m	±0.02	$\Omega R/V_\infty$	±0.001
C_D	±0.1	α	±0.1°
C_L	±0.1	θ_0	±0.5°[1]
C_Y	±0.07	θ_1	±0.1°
L/D	±0.05	θ_2	±0.1°

[1] The uncertainty noted for θ_0 is a combination of uncertainties in establishing the zero reference ($(\Delta\theta_0)_{ZERO}$) and in measuring differences from that zero reference ($(\Delta\theta_0)_{SENSITIVITY}$). These two quantities were estimated to be as follows:

$$(\Delta\theta_0)_{ZERO} = \pm0.4°$$
$$(\Delta\theta_0)_{SENSITIVITY} = \pm0.1°$$

In general, repeatability of the force data was well within the maximum uncertainties indicated.

RESULTS AND DISCUSSION

The results of the tests reported herein are presented graphically in figures 6 through 17. Data were taken at $M_\infty^* = 1.62$, 2.42 and 3.54; but because the variations in aerodynamic characteristics over this Mach number range are small and essentially linear, only the data for the highest and lowest Mach numbers are presented. The discussion of these results is divided into three sections: (1) rotor operating characteristics, $\Omega R/V_\infty$ vs. θ_O, (2) vehicle aerodynamic characteristics, and (3) cyclic pitch control characteristics. The body-alone aerodynamic characteristics are included as part of (2).

Rotor Operating Characteristics

The effects of angle of attack on the rotor operating characteristics for the elliptic and double-wedge blade configurations are shown in figures 6 and 7, respectively. For all supersonic test conditions, the variation of dimensionless rotor tip speed $\Omega R/V_\infty$ with blade pitch (θ_O) is nearly linear and the slope increases with angle of attack. The slopes of the curves for the double-wedge blades are greater than those for the elliptic blades because of the lower section profile drag at supersonic speeds. No difficulties were encountered in controlling rotor speed through manual control of blade pitch.

To illustrate typical rotor speed variations which a rotor entry vehicle might encounter, the rotor tip speed has been plotted for various Mach numbers in figures 8 and 9. Tip speed variations are presented for fixed blade pitch at two angles of attack for both elliptic (fig. 8) and double-wedge (fig. 9) blade configurations. The subsonic and transonic data were taken from references 8 and 9. For a given vehicle attitude the data indicate no large changes in rotor speed with flight Mach number in the supersonic range ($M_\infty \geqslant 1.62$). Strangely, the speed range that appears most likely to present rotor speed control problems is the low subsonic speed range where transition between stalled and unstalled rotor operation caused very large changes in rotor speed (see ref. 8).

Vehicle Aerodynamic Characteristics

Capsule body- The longitudinal characteristics of the body-alone are presented in figure 10 for Mach numbers 1.62 and 3.54. For both Mach numbers the maximum drag coefficient is about 1.3 and maximum lift-drag ratio is about 0.7. With the present moment center location, the body is nearly trimmed and has almost neutral static margin over a wide angle-of-attack range which includes the angles for maximum L/D, $\alpha = 40°$, and maximum lift, $\alpha = 50°$.

Body plus rotor- The longitudinal aerodynamic characteristics along with side-force and rolling-moment coefficients and dimensionless tip speed for the complete rotor vehicle are presented in figures 11 and 12 for the elliptic and double-wedge blade configurations, respectively. Differences between the aerodynamic characteristics for the two configurations are small. The dimensionless tip speed, however, is markedly different as discussed previously. Differences in lift, drag, pitching moment, and side force due to changes in blade pitch angle, θ_O, are likewise small.

The addition of the rotor to the body produced fairly large amounts of lift, drag, and pitching moment. In axial flight ($\alpha = 90°$) where the rotor acts merely as a decelerator, the total drag is about 2.5 times that of the body. This drag increase is roughly in proportion to the increase in the projected blade area normal to the wind. In an undisturbed flow the rotor should produce more force per unit cross-sectional area than the body because it resembles a two-dimensional surface (aspect ratio $\cong 9$). However, the influence of the body flow field decreases the airload on the rotor. (See section on Body interference.)

The maximum lift-drag ratio varies from 0.75 at $M_\infty = 1.62$ to 0.68 at $M_\infty = 3.54$ and occurs at an angle of attack of about 27°. Because of the disproportionate sizing of the hub and blade retention system on the model, these L/D values are unrealistically low for a full-scale machine. The estimated effect of the hub and grips on the lift-drag ratio is discussed in a later section. The pitching moments produced by the rotor are especially large in the intermediate angle-of-attack range, making the model statically unstable at angles of attack up to 50° and rendering it out of trim. Flaps were added to the body to provide pitch trim, and the results are discussed in a later section.

The rotor produced substantial rolling moments that were quite sensitive to collective pitch changes. The highest rolling moments measured occurred at $M_\infty = 1.62$. The variations of rolling moment with angle of attack reach a maximum at between 60° and 70°. The variation of rolling moment was such that roll trim occurred in the glide attitude where maximum L/D occurs. Hence little additional roll trim would be needed for flight at maximum L/D. In addition to the rolling moment, some side force is produced by the rotor but it remained small compared to the lift.

Body interference- To determine approximately the effects of the body flow field on rotor performance, the elliptic-blade rotor was operated behind a pointed cone-cylinder (fig. 2(d)). The cone-cylinder acted merely as a fairing for the hub and blade pitch control mechanism. This test was conducted only in the angle-of-attack range from 63° to 90° where the cone-cyclinder would produce much less flow field disturbance than the blunt capsule. Rotor lift and drag coefficients from this test are compared with the blunt capsule in figure 13. In both cases the forebody-alone forces have been removed, leaving rotor-plus-interference forces. Section lift and drag characteristics of the rotor blade airfoil (ref. 12) have been included for comparison and all the data are referenced to the capsule area. The data indicate that large reductions in lift and drag result from flow field interference by the capsule at large angles of attack. The rotor operating in the cone flow field gave forces remarkably close to the rotor blade airfoil data.

Pitch trim flaps- During an early phase of testing it became apparent that the rotor produced pitching moments too large to be trimmed by the available cyclic pitch controls. The flaps illustrated in figure 2(c) were then added to provide trim. Flap area and deflection requirements for trim at $\alpha = 30°$ and $M_\infty = 3.5$ were estimated by Newtonian theory to predict the pressure on the windward flap surfaces. The flaps were contoured to represent a section of the capsule surface and were mounted in a position representing 180° deflection. Pitching-moment results of the flap tests are shown with the basic data in figure 14 for Mach numbers 1.62 and 3.54. The flaps proved to be quite effective for trim at supersonic speeds and even eliminated the static instability at $M_\infty = 3.54$. Data not shown indicate that about neutral stability persists to $M_\infty = 2.5$ with the flaps extended.

Effect of hub and blade grip forces- To evaluate the effect of the hub and blade grips on lift-drag ratio, theoretical body forces were calculated by Newtonian theory and added to experimental rotor forces. The experimental rotor forces were obtained by subtracting data obtained for the model with the blades removed (grips and hub rotating) from the body-plus-rotor data (fig. 11(b)). Autorotation of the hub and grips was sustained without blades by application of -20° collective pitch. The resulting lift-drag ratios are presented with the test data for $M_\infty = 3.54$ in figure 15. The comparison is made only for the highest test Mach number because the application of the theory at the lower test Mach numbers is questionable. At this Mach number, the maximum lift-drag ratio is increased by 50 percent when the hub and grip forces are removed.

Effects of sting inclination- Discontinuities in the data for angles of attack between 27° and 33° and between 60° and 63°, (figs. 11 and 12) appear to be caused by sting interference. The lift and rolling moment are affected most and the effects are greatest at $M_\infty = 1.62$; least at $M_\infty = 3.54$. Because of the different mounting arrangements used (see fig. 4), testing at $\alpha = 63°$ placed the sting at 27° inclination to the free stream whereas at $\alpha = 60°$ the sting was parallel to it. Therefore, at $\alpha = 60°$ the data are expected to be more reliable than at $\alpha = 63°$. For the angles of attack 27° and 33°, the inclination of the sting to the free stream is the same so that the data for neither angle of attack can be thought of as the more reliable.

Cyclic Pitch Control Characteristics

The variations of side force, rolling moment and pitching moment coefficients and the lift-drag ratio with sine and cosine feathering amplitudes (θ_1 and θ_2, respectively) are presented in figures 16 and 17 for the elliptic and double-wedge blade configurations, respectively. Included are data for six angles of attack and several collective blade pitch angles obtained at Mach numbers 1.62 and 3.54. Control power is indicated by the slopes of the rolling moment and pitching moment curves. The data for the range of glide angles of attack indicate that the sine feathering provides mostly roll control with little pitch control and vice versa for the cosine feathering. It is apparent then that the control system would need some built-in phasing in order to isolate roll control from pitch control. The amount of control phasing needed could be determined from these moment curves but it would not be applicable to a vehicle of different size or for blades having different inertial characteristics. Experimental determination of control phasing can be accomplished only with the full-size machine. An attempt to use classical rotor theory to predict the control phasing for the model was not successful.

The roll control provided by sine feathering was sufficient to trim the model in glide flight near maximum L/D. However, neither component of feathering could provide sufficient pitching moment for longitudinal trim; hence pitch flaps were needed as described previously.

The effects of cyclic pitch on the lift-drag ratio were not too significant. Generally, cosine feathering had almost no effect on L/D and sine feathering in the direction needed for roll trim tended to increase L/D.

CONCLUSIONS

Wind-tunnel tests have been conducted on two configurations of a rotor entry vehicle model to establish unpowered-rotor operating and aerodynamic characteristics at Mach numbers from 1.62 to 3.54. The tests were conducted using two different rotor blade sections, a 20-percent-thick modified ellipse and a 20-percent-thick double wedge. The rotor diameter was three times the body diameter. Collective blade pitch was used to control rotor speed at all model attitudes. The effectiveness of blade cyclic pitch and body-mounted pitch flaps for trimming was also determined.

The results of this investigation indicate the following conclusions:

1. The rotor speed characteristics were regular and controllable by manually operated blade pitch controls. No sudden variations in rotor speed occurred at supersonic speed.

2. The maximum lift-drag ratio varied from 0.75 at Mach number 1.62 to 0.68 at Mach number 3.54, but these values are unrealistically low because of the oversized hub and blade retention system of the model.

3. The rotor produced large amounts of lift, drag, and pitching moment. These characteristics were not significantly affected by either collective blade pitch variation or blade airfoil section.

4. Large pitching moments were produced by the rotor. In the glide attitudes the basic model configurations were statically unstable and out of trim. Cyclic blade pitch controls were not adequate for trimming out these pitching moments. Adding flaps to the body provided the needed trim and also eliminated the instability at Mach numbers of 2.5 and higher.

5. Cyclic pitch controls were found to be quite satisfactory for trimming the rotor rolling moment at glide attitudes (15° to 27° angle of attack) and did not adversely affect the lift-drag ratio.

6. The influence of the body flow field substantially reduced the lift and drag of the rotor.

Ames Research Center
National Aeronautics and Space Administration
Moffett Field, Calif., 94035, Sept. 15, 1970

REFERENCES

1. Haig, C.R. Jr.: The Use of Rotors for the Landing and Reentry Braking of Manned Spacecraft. IAS Paper No. 60-17, Jan. 1960.

2. Fletcher, C. J.; and Tesch, E. C., Jr.: ROR-Chute Concept for Systems. Thiokol Chemical Corp. TR 3740, Jan. 1961.

3. Kretz, M.: Application of Rotary Wing Techniques to Atmospheric Re-Entry and Launch Vehicle Recovery Problems. Paper presented at the European Symposium on Space Technology, London, England, June 1961.

4. Barzda, J. J.; and Schultz, E. R.: Test Results of Rotary-Wing Decelerator Feasibility Studies for Capsule Recovery Applications. SAE Paper No. 756D, Sept. 1963.

5. Ham, Norman D.: An Experimental and Theoretical Investigation of a Supersonic Rotating Decelerator. J. Am. Helicopter Soc. vol. 8, no. 1, Jan. 1963. pp. 8-18.

6. Levin, Alan D.; and Smith, Ronald C.: An Analytical Investigation of the Aerodynamic and Performance Characteristics of an Unpowered Rotor Entry Vehicle. NASA TN D-4537, 1968.

7. Smith, Ronald C.; and Levin, Alan D.: Heat-Transfer Measurements on the Rotor Blade of a Rotor Entry Vehicle Model. NASA TN D-4065, 1967.

8. Smith, Ronald.; and Levin, Alan D.: Experimental Aerodynamic Performance Characteristics of a Rotor Entry Vehicle Configuration – I, Subsonic. NASA TN D-7046

9. Levin, Alan D.; and Smith, Ronald C.: Experimental Aerodynamic Performance Characteristics of a Rotor Entry Vehicle Configuration – II, Transonic. NASA TN D-7047

10. Hollrock, Richard: Re-Entry Rotor Tested. Verti-Flite, Feb. 1967. pp. 31-2.

11. Huntsberger, Ralph R.; and Parsons, John F.: The Design of Large High-Speed Wind Tunnels. AGARD 4th Assembly, Schwernigen, Netherlands, AG 15/p 6, May 1954.

12. Randall, Greenfield A., Jr.: Aerodynamic Characteristics of Two 20 Percent Thick, Rectangular Wings up to 90° Angle of Attack at Subsonic, Transonic and Supersonic Speeds. NASA CR-73097, April 1967. Aerostructures Inc.

TABLE 1.- SCOPE OF THE BODY-ROTOR INVESTIGATION

	PART I		PART II		PART III	
Config. \ Mach No.	0.3	0.7	0.9	1.1	1.6	3.5
B	○	○	○	○	○	○
BR_d	○	○	○	○	○	○
$BR_e{}^L$	○	○	○	○		
BR_e	○	○	○	○	○	○

Configuration code:

- B - Body
- R_d - Short double-wedge blade section (R/d = 1.5)
- $R_e{}^L$ - Long elliptic-blade section (R/d = 2.0)
- R_e - Short elliptic-blade section (R/d = 1.5)

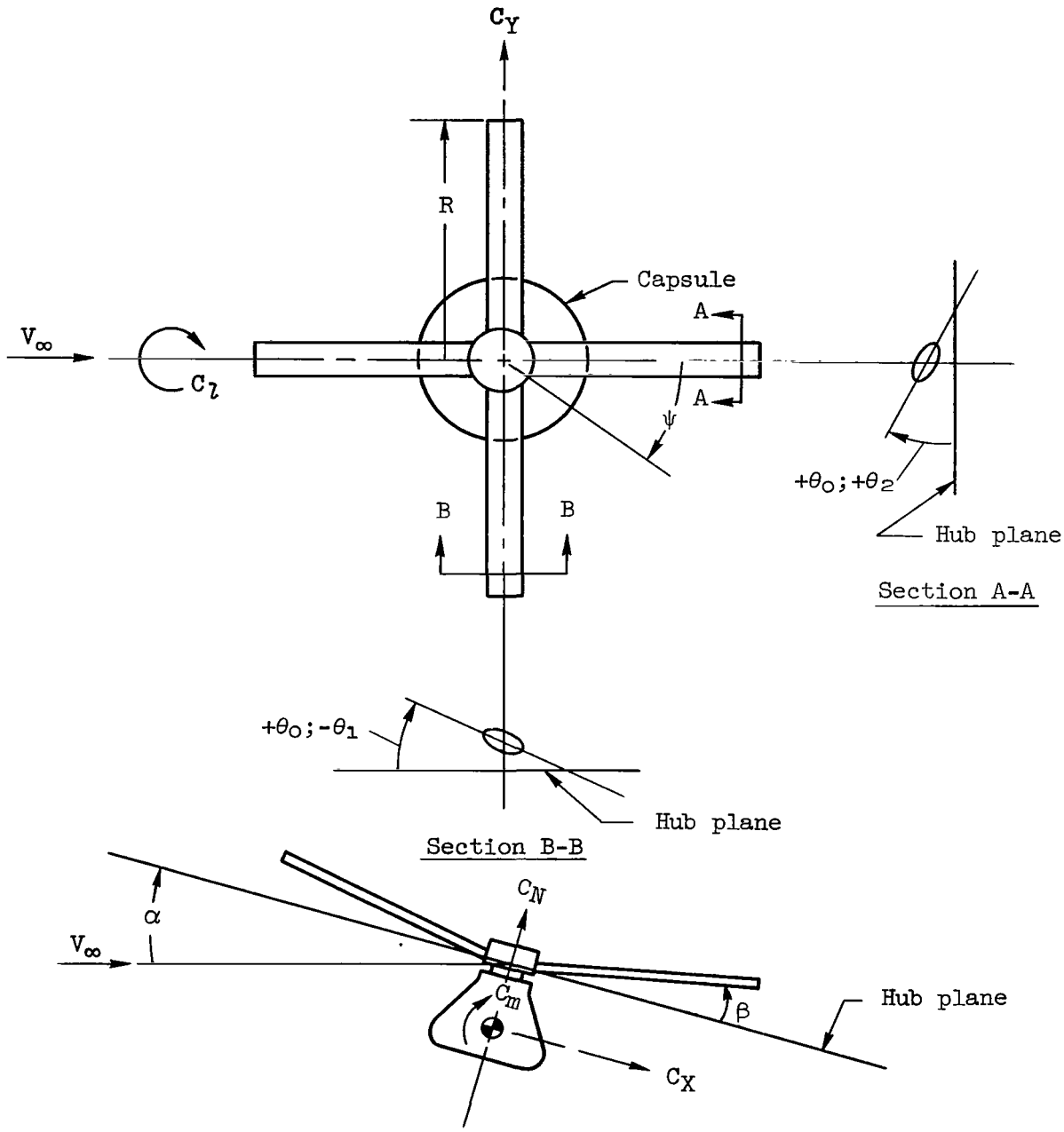

Figure 1.- Notation showing direction of forces and angles.

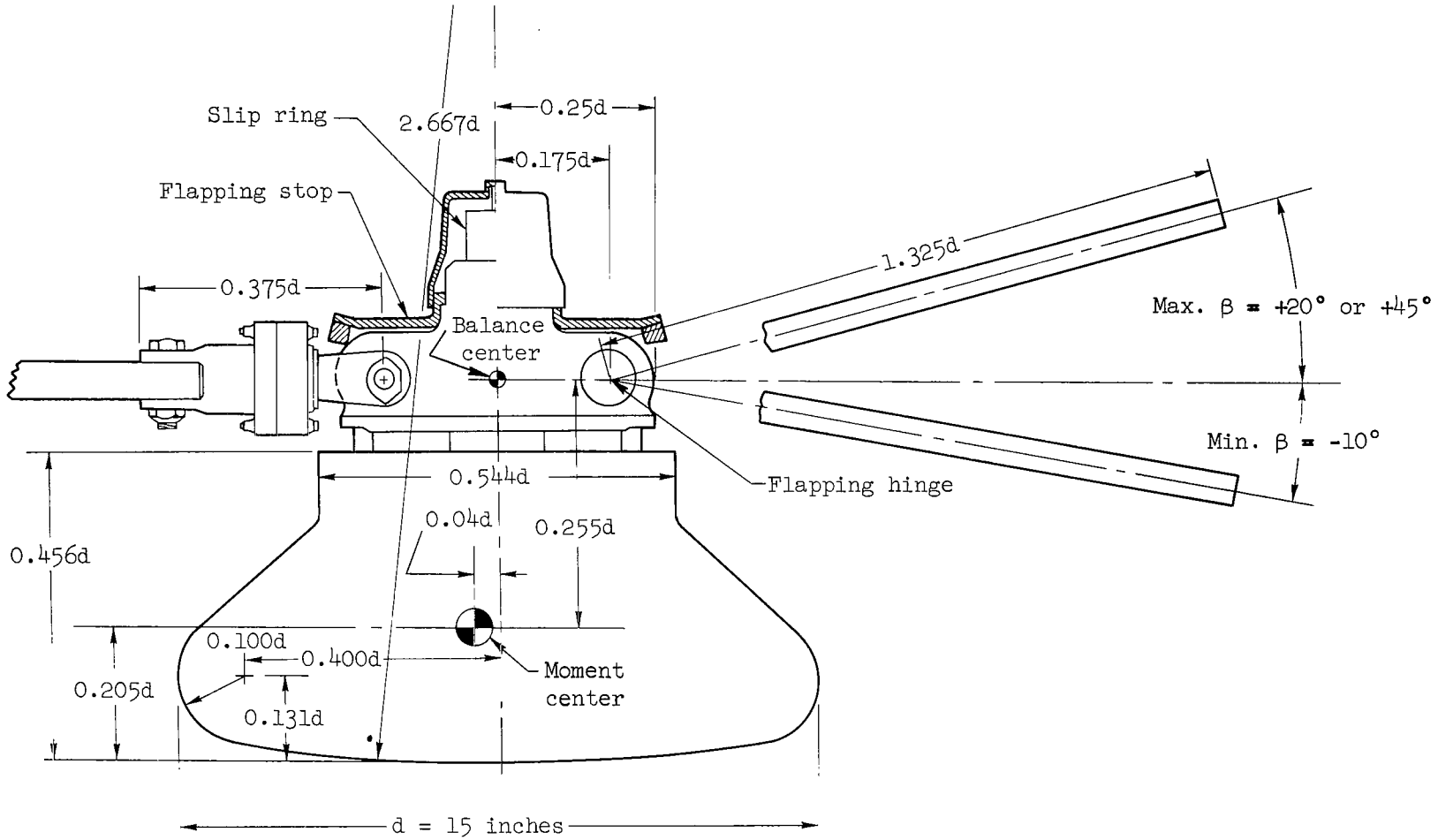

(a) Body and hub geometry

Figure 2.- Model details.

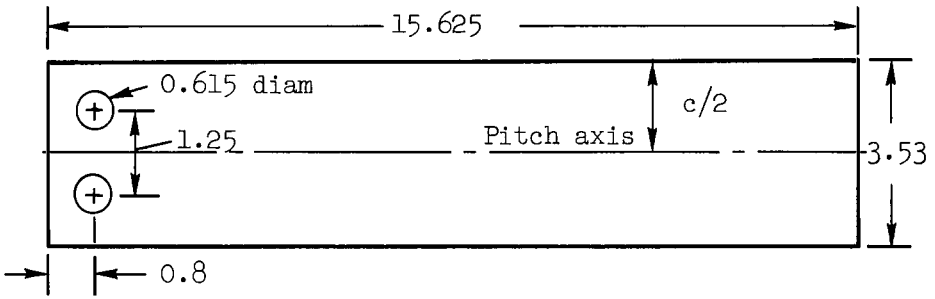

Note: All dimensions are in inches

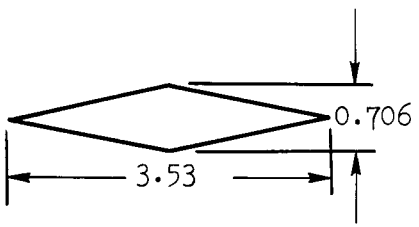

Wedge section

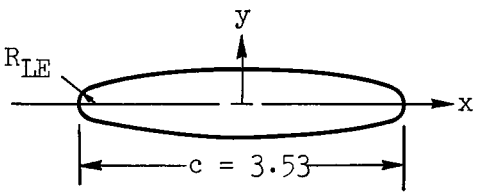

Modified ellipse section

MOD. ELLIPSE COORDINATES	
± x/c	± y/c
0	0.1000
0.0417	0.0994
0.0834	0.0985
0.1250	0.0969
0.1667	0.0950
0.2083	0.0925
0.2500	0.0890
0.2917	0.0840
0.3333	0.0777
0.3750	0.0702
0.4167	0.0606
0.4583	0.0481
0.4688	0.0440
0.4792	0.0388
0.4896	0.0299

(b) Rotor blade sections and planform

Figure 2.- Continued.

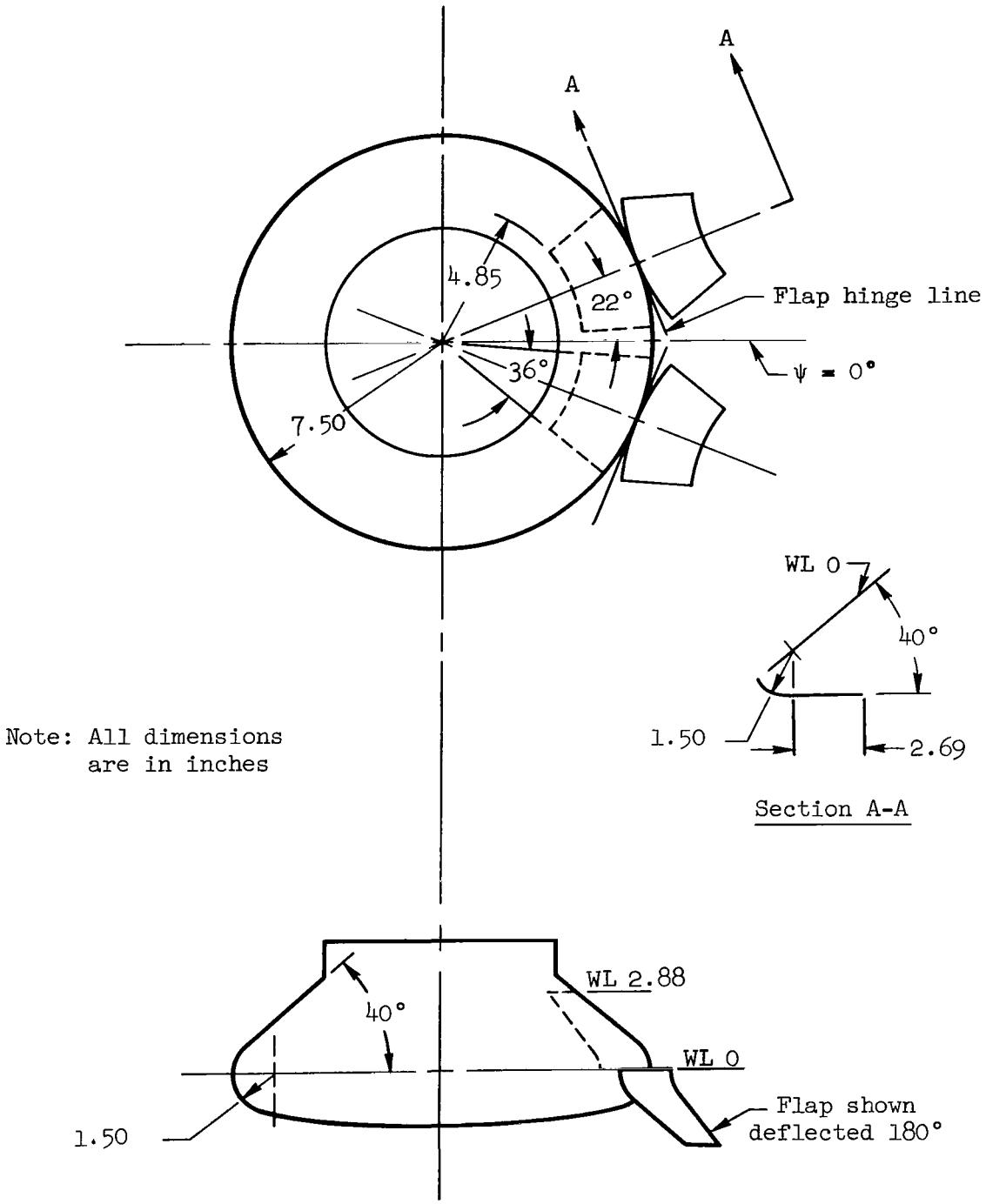

(c) Pitch flap geometry

Figure 2.- Continued.

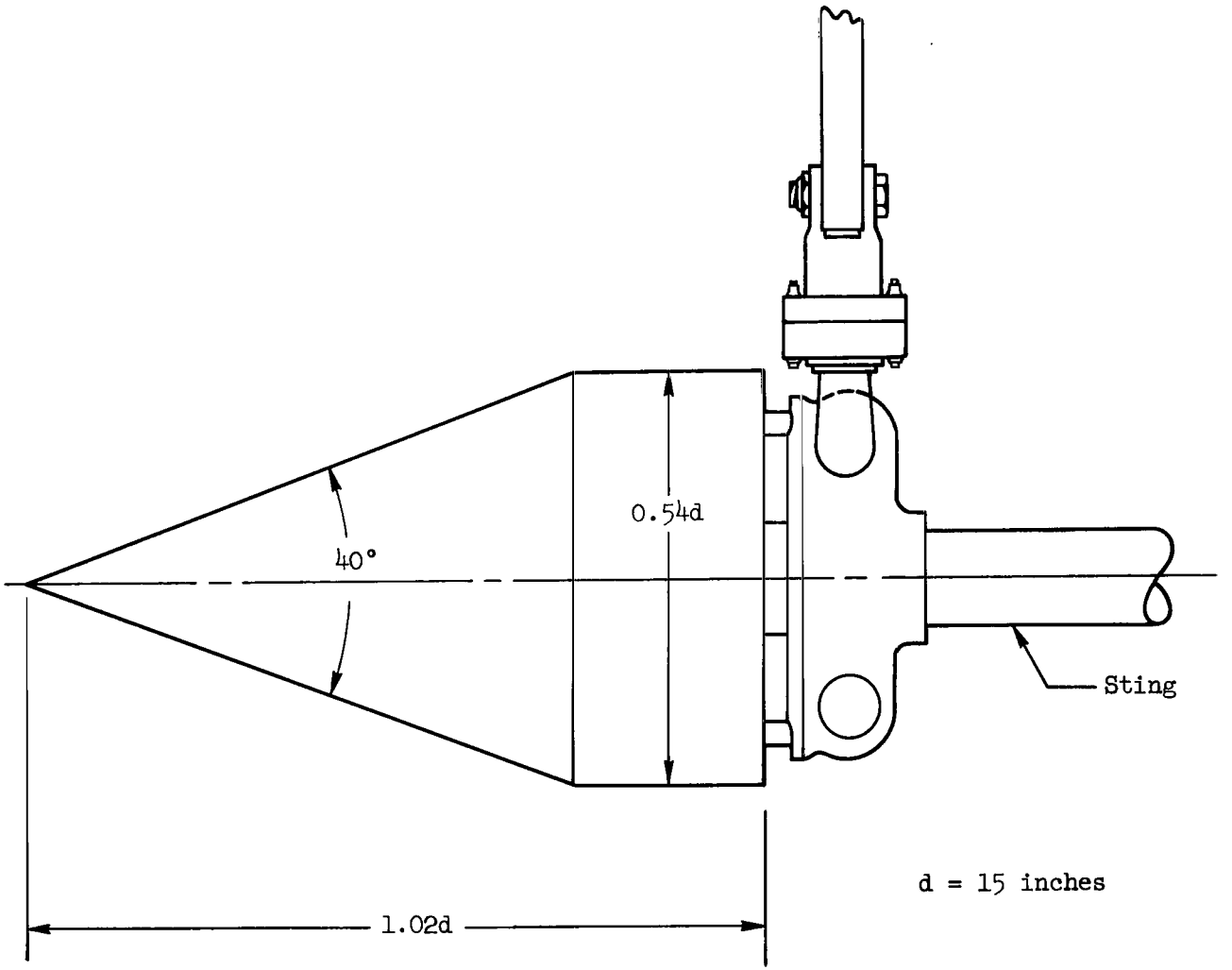

(d) Cone forebody geometry

Figure 2.- Concluded.

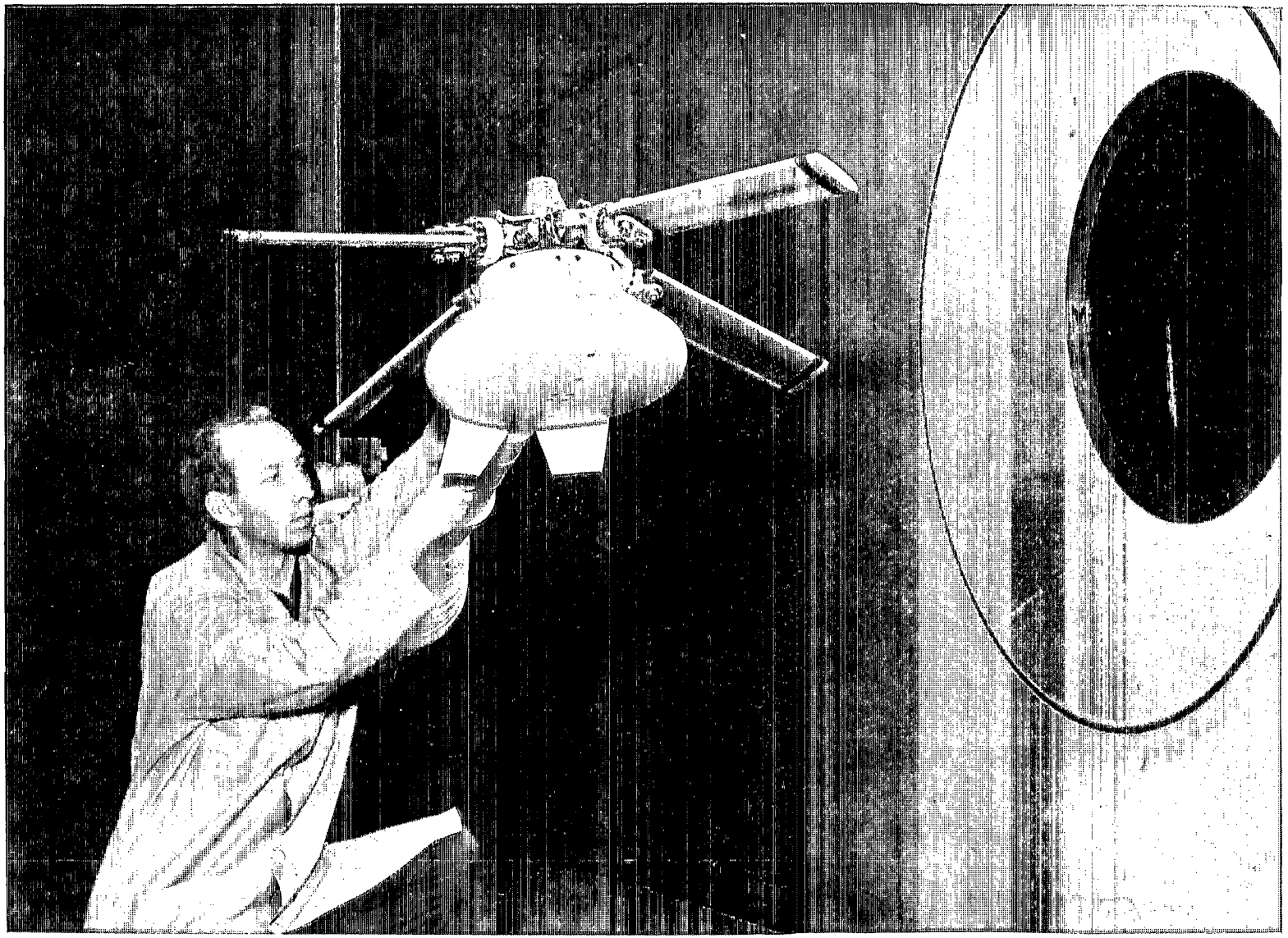

(a) 8- by 7-Foot Wind Tunnel.

Figure 3.- Model mounted in wind tunnel.

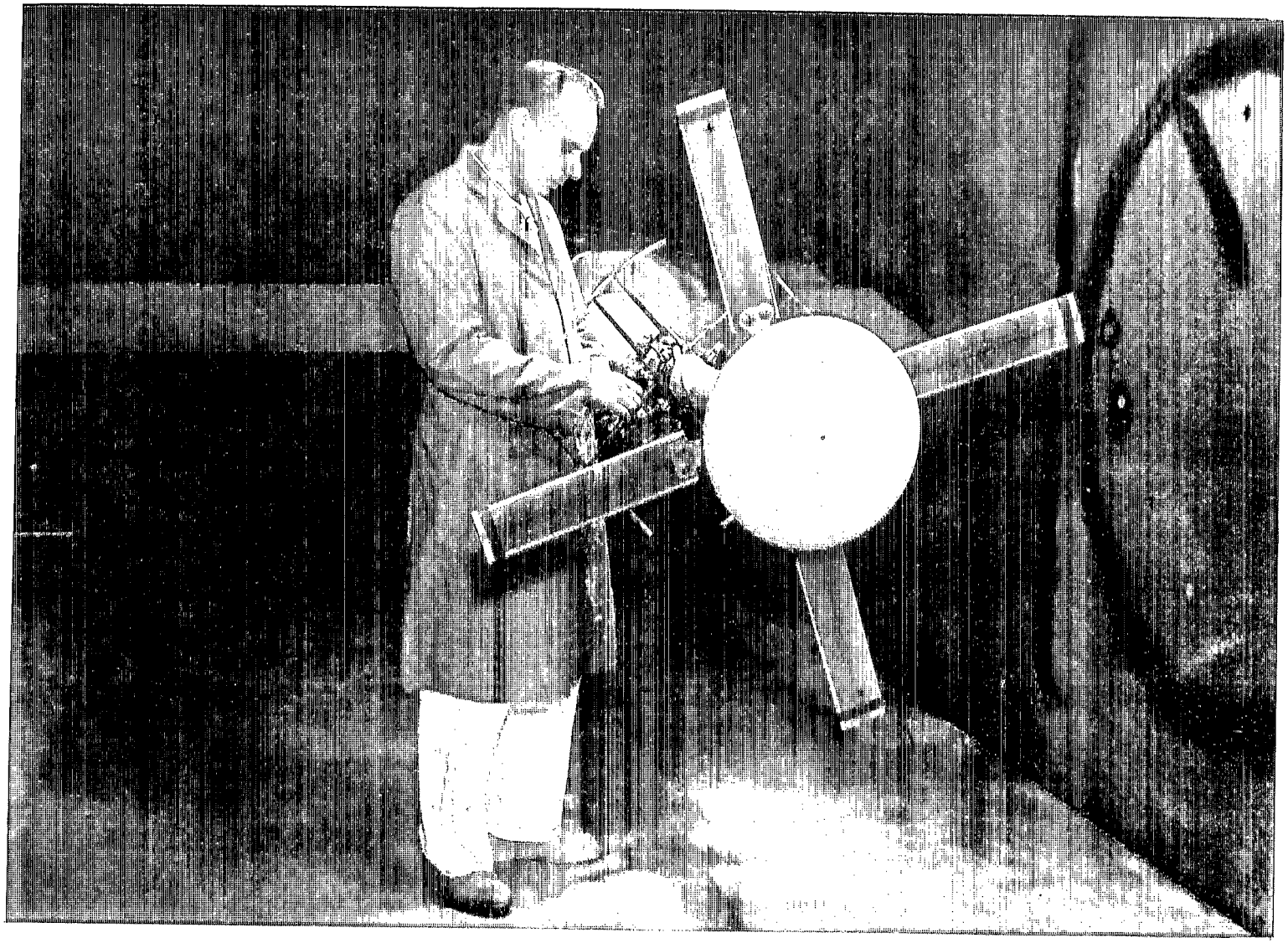

(b) 9- by 7-Foot Wind Tunnel.

Figure 3.- Continued.

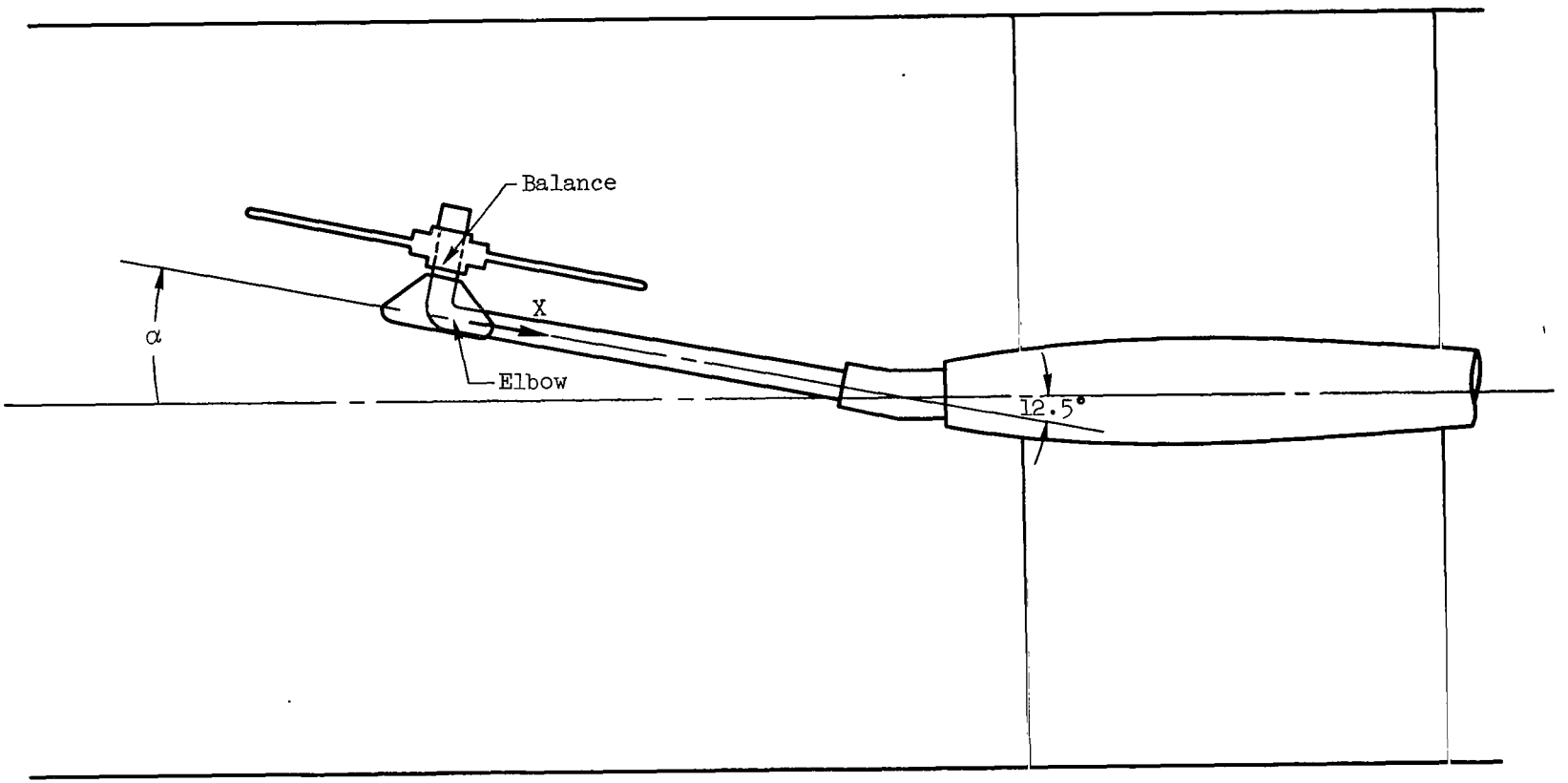

(a) $\alpha = 0^{\circ}$ to 27°

Figure 4.- Model mounting arrangements.

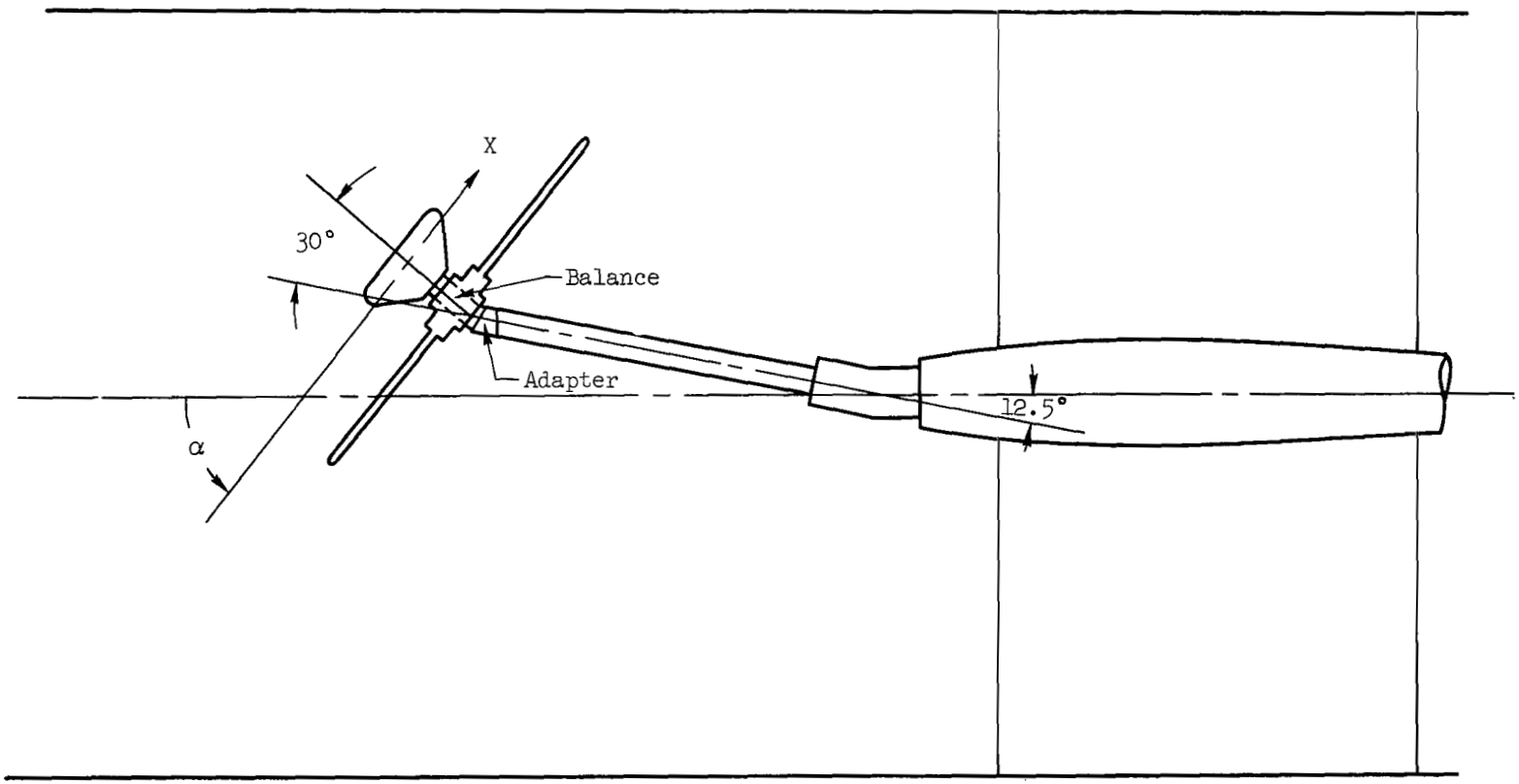

(b) $\alpha = 33^{\circ}$ to 60°

Figure 4.- Continued.

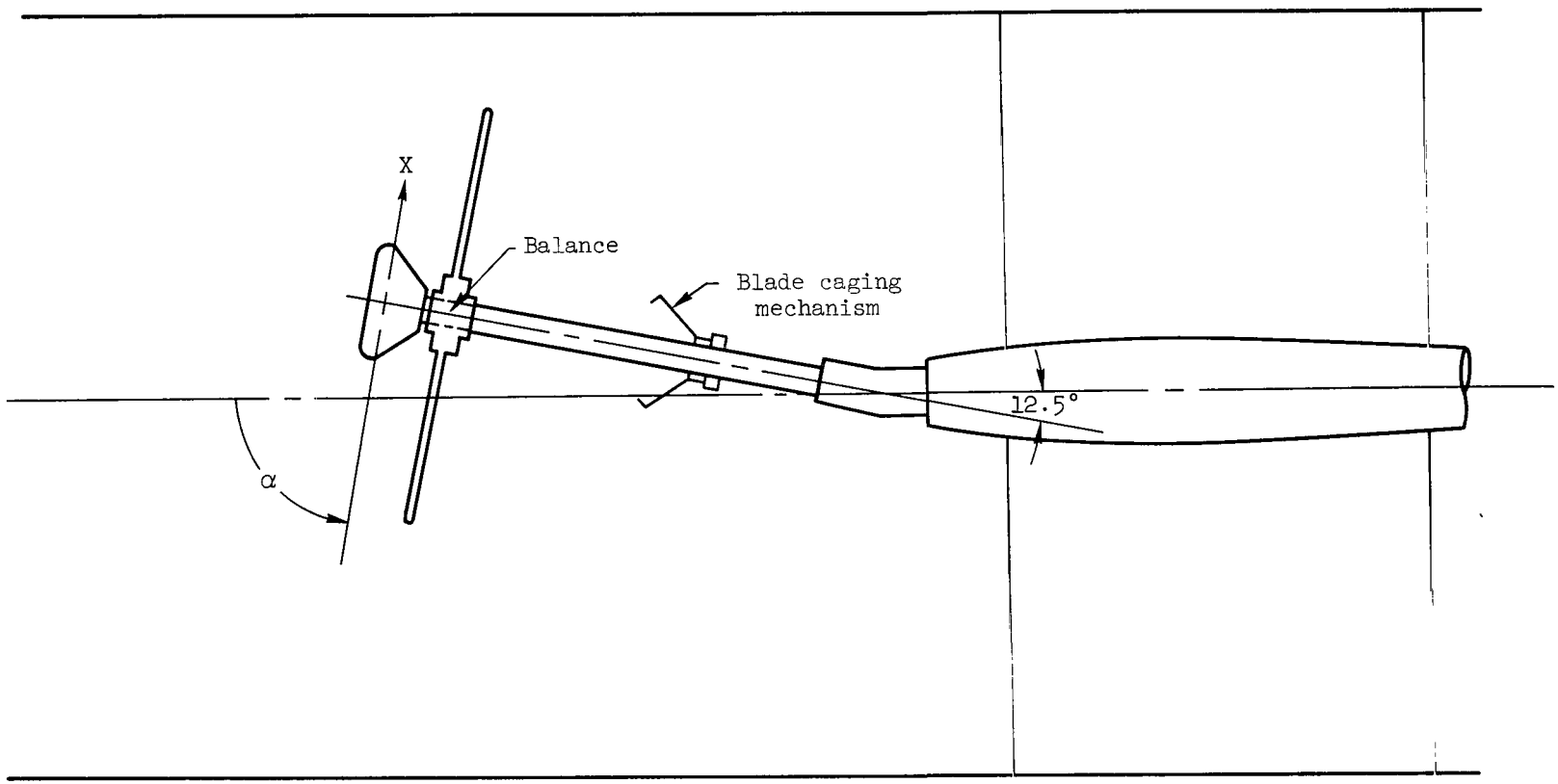

(c) $\alpha = 63^{\circ}$ to 90°

Figure 4.- Concluded.

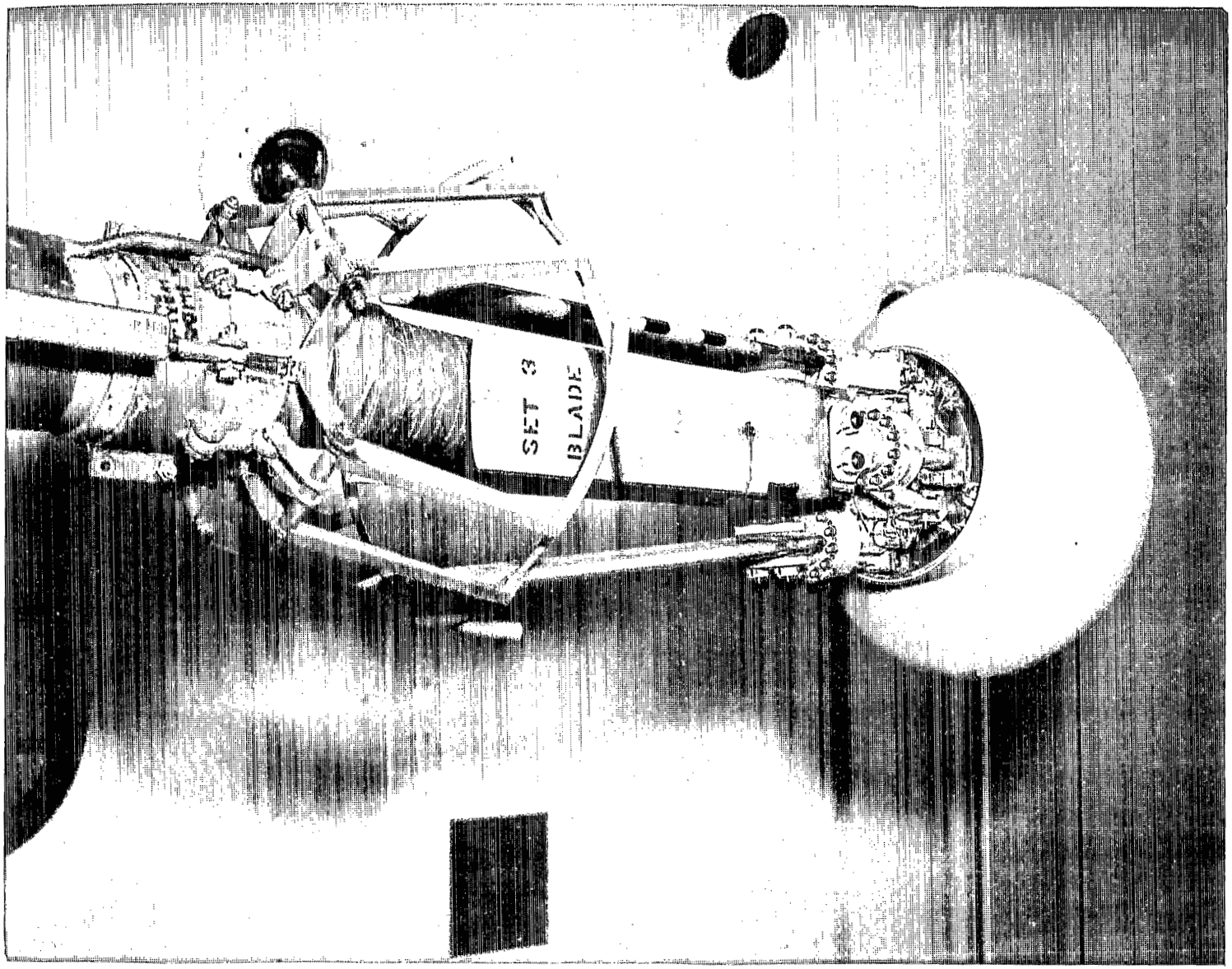

Figure 5.- Model with rotor blades in the caged position.

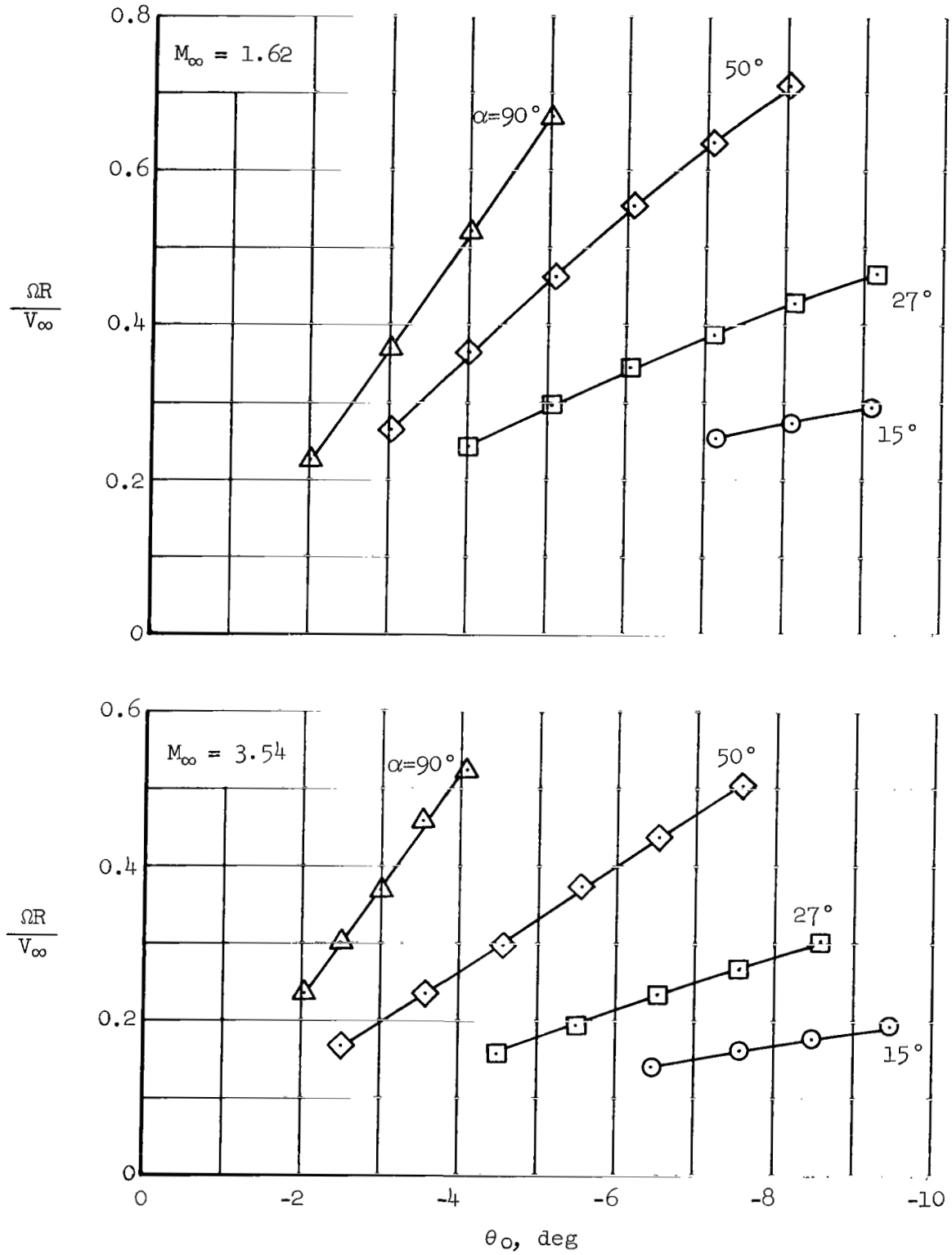

Figure 6.- Rotor operating characteristics, elliptic blades; $\theta_1 = 0^o$, $\theta_2 = 0^o$.

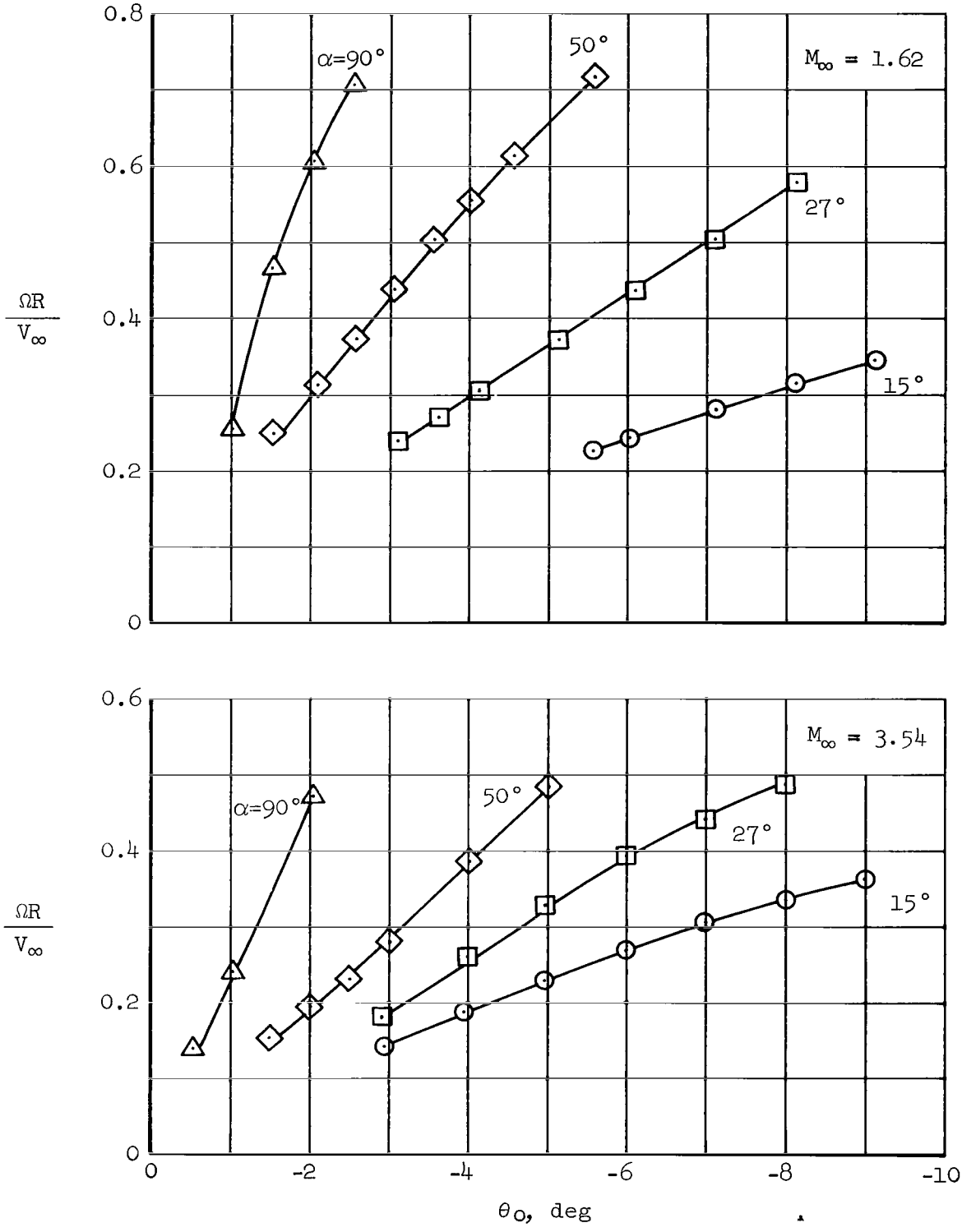

Figure 7.- Rotor operating characteristics, double-wedge blades; $\theta_1 = 0^\circ$, $\theta_2 = 0^\circ$.

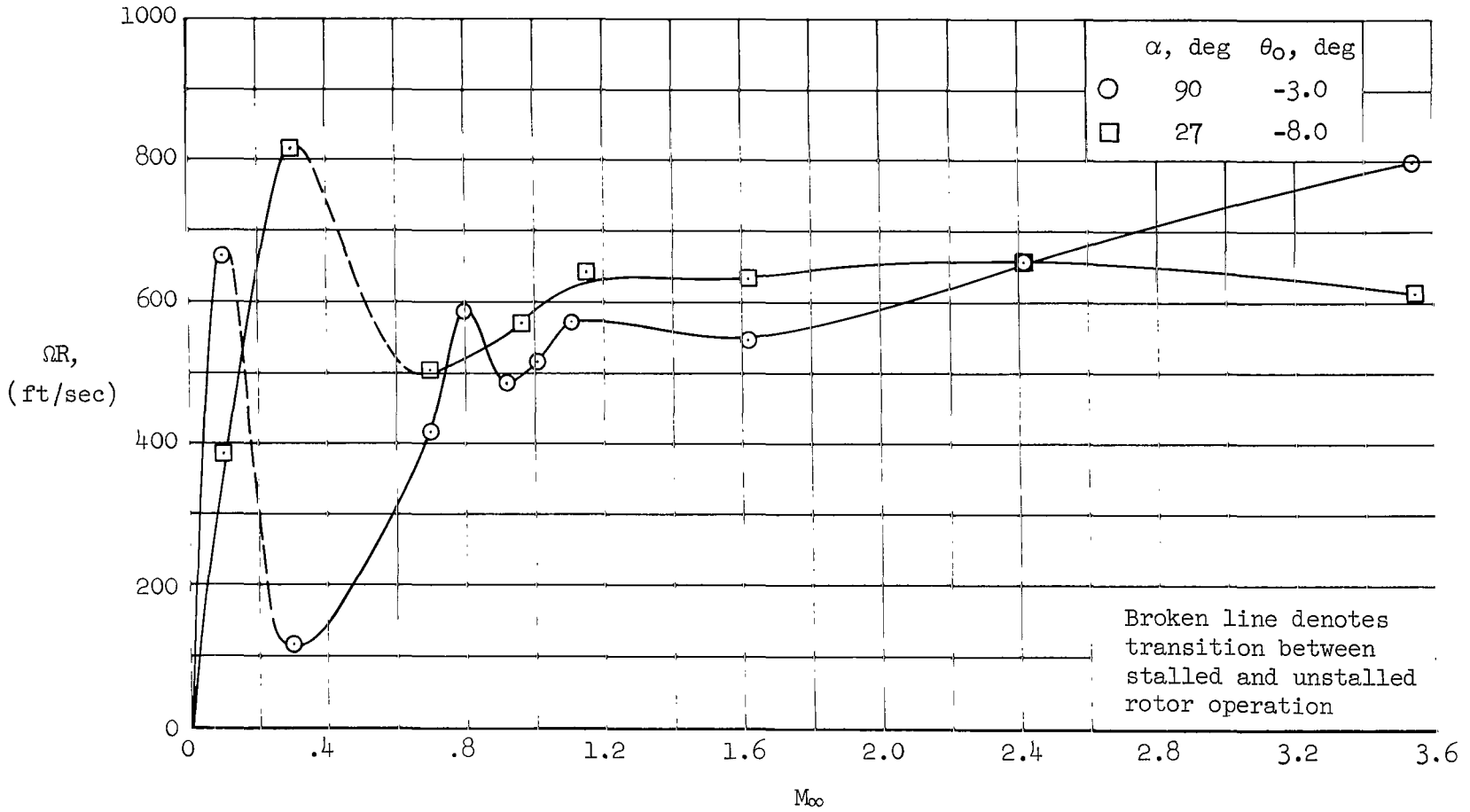

Figure 8.- Variations of rotor tip speed with Mach number for elliptic blades; $\theta_1 = 0^\circ$, $\theta_2 = 0^\circ$.

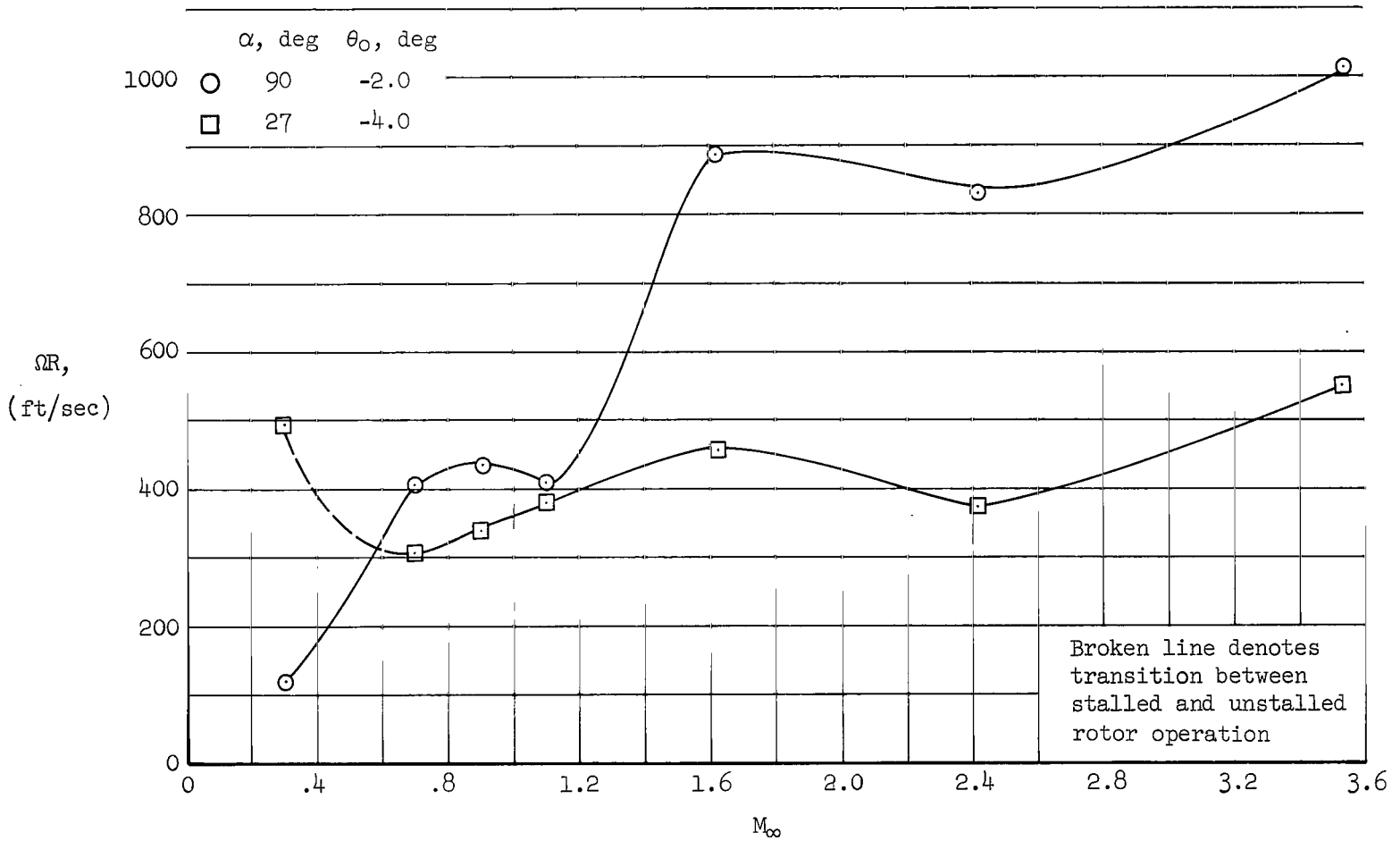

Figure 9.- Variations of rotor tip speed with Mach number for double-wedge blades; $\theta_1 = 0^o$, $\theta_2 = 0^o$.

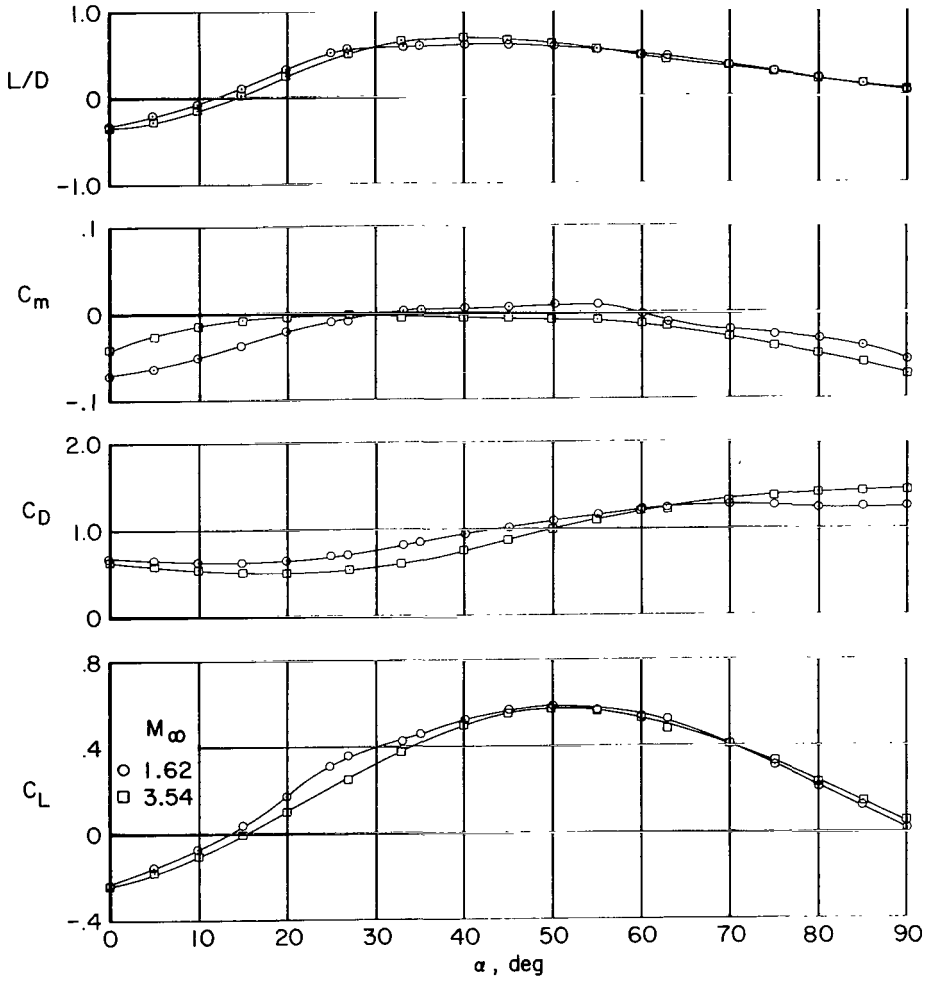

Figure 10.- Aerodynamic characteristics of the body-alone.

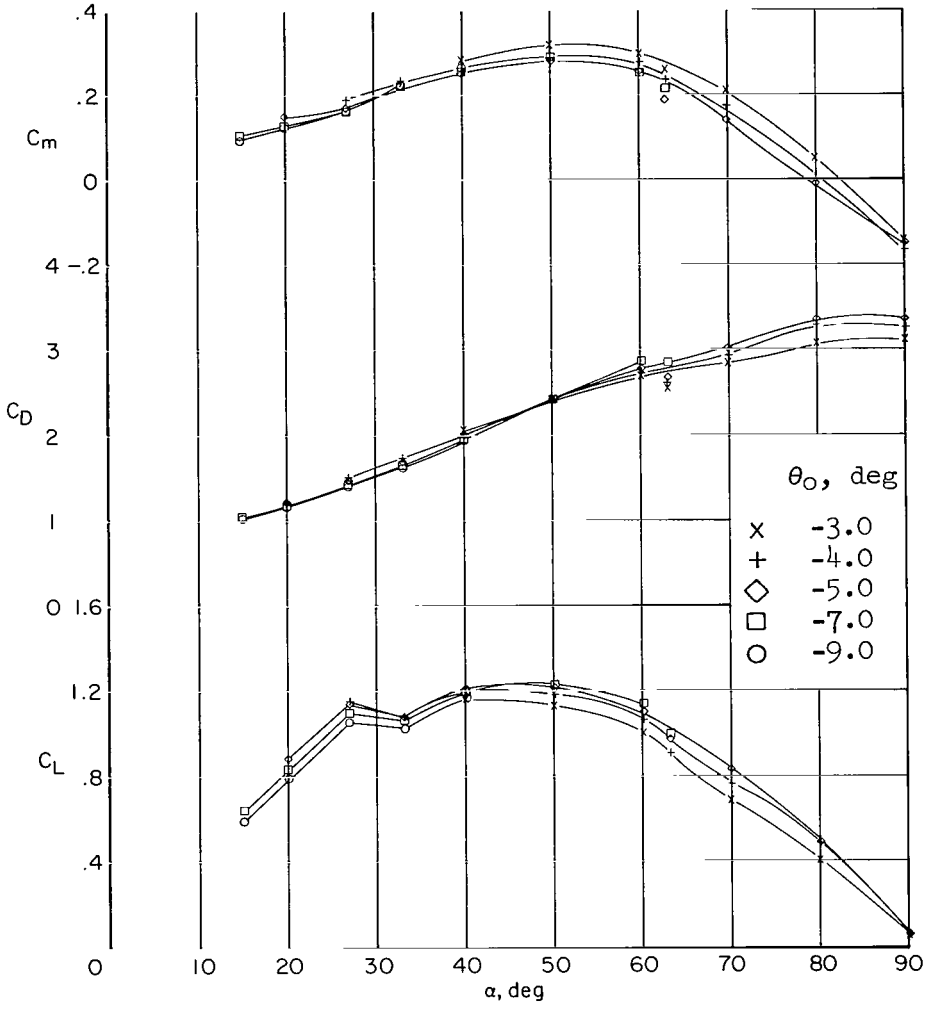

(a) $M_\infty = 1.62$

Figure 11.- Aerodynamic characteristics of the elliptic-blade configuration; $\theta_1 = 0^o$, $\theta_2 = 0^o$.

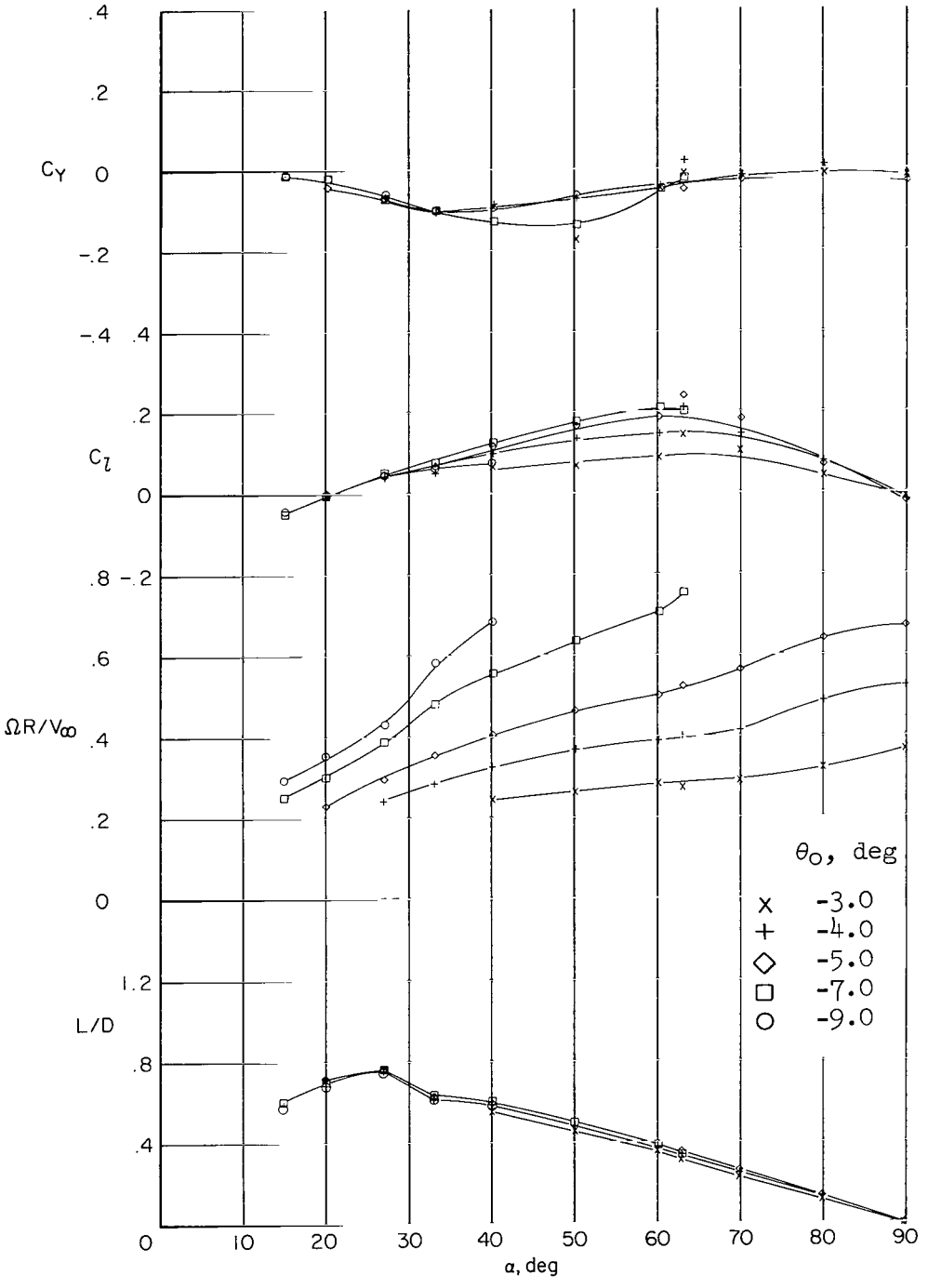

(a) M_∞ = 1.62 - Concluded.

Figure 11.- Continued.

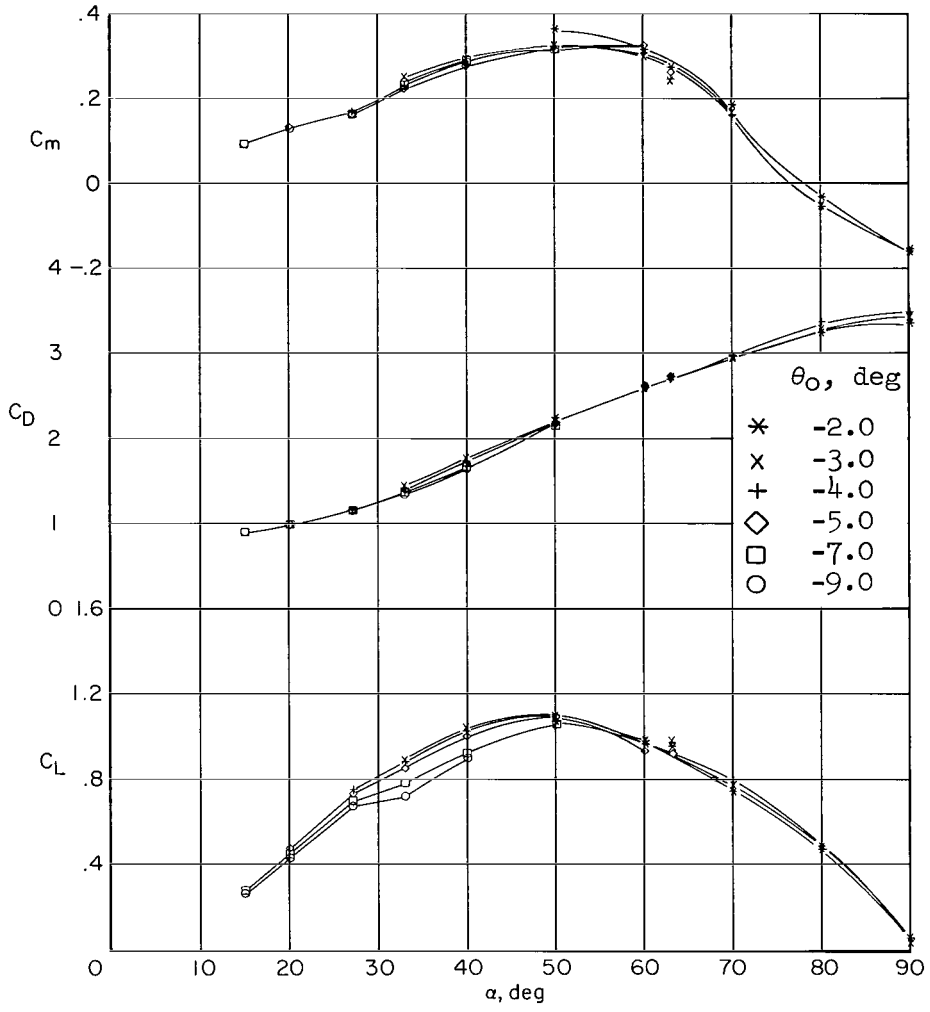

(b) $M_\infty = 3.54$

Figure 11.- Continued.

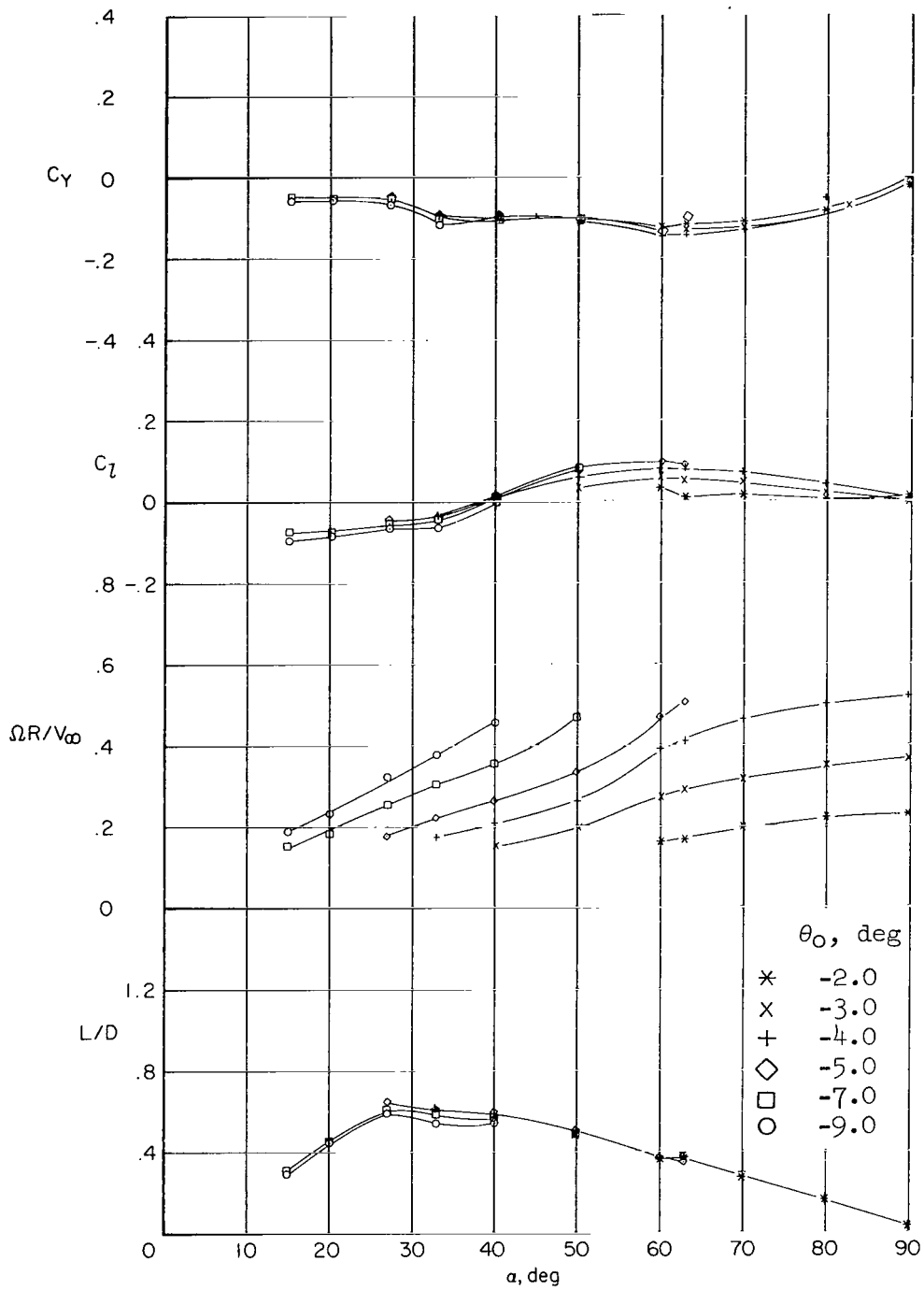

(b) $M_\infty = 3.54$ - Concluded.

Figure 11.- Concluded.

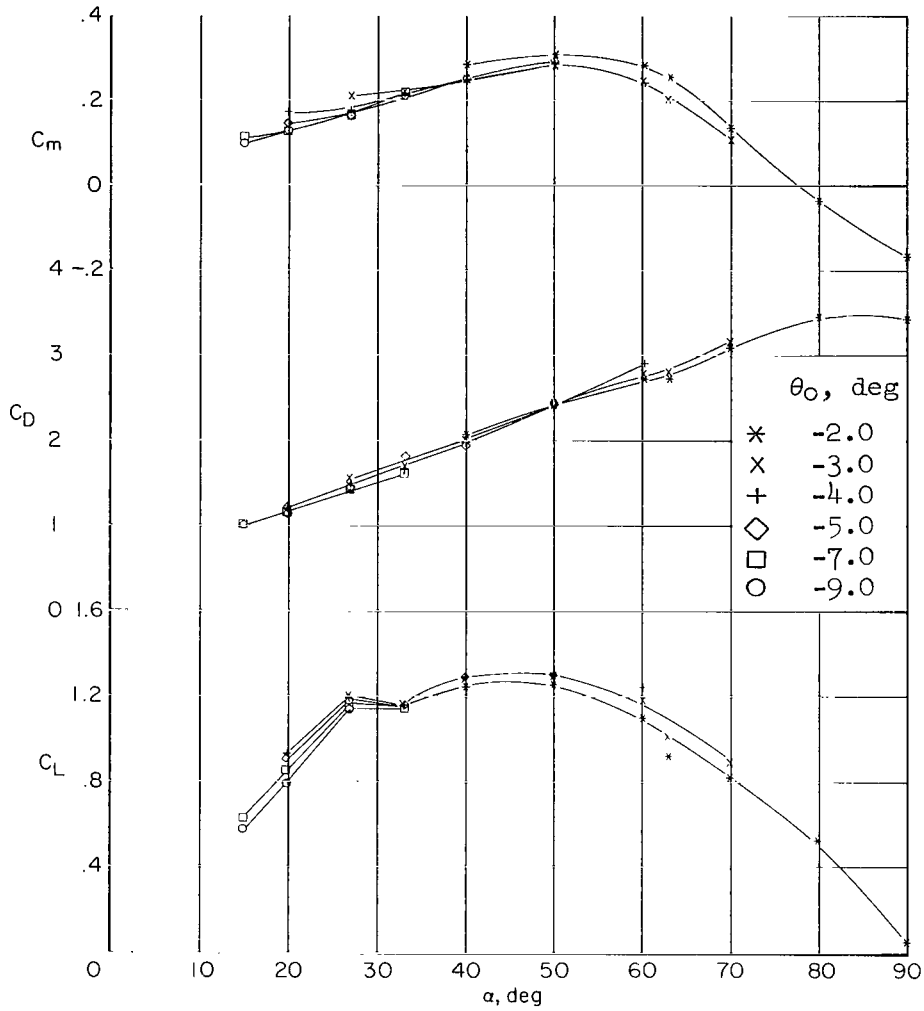

(a) $M_\infty = 1.62$

Figure 12.- Aerodynamic characteristics of the double-wedge blade configuration; $\theta_1 = 0^o$, $\theta_2 = 0^o$.

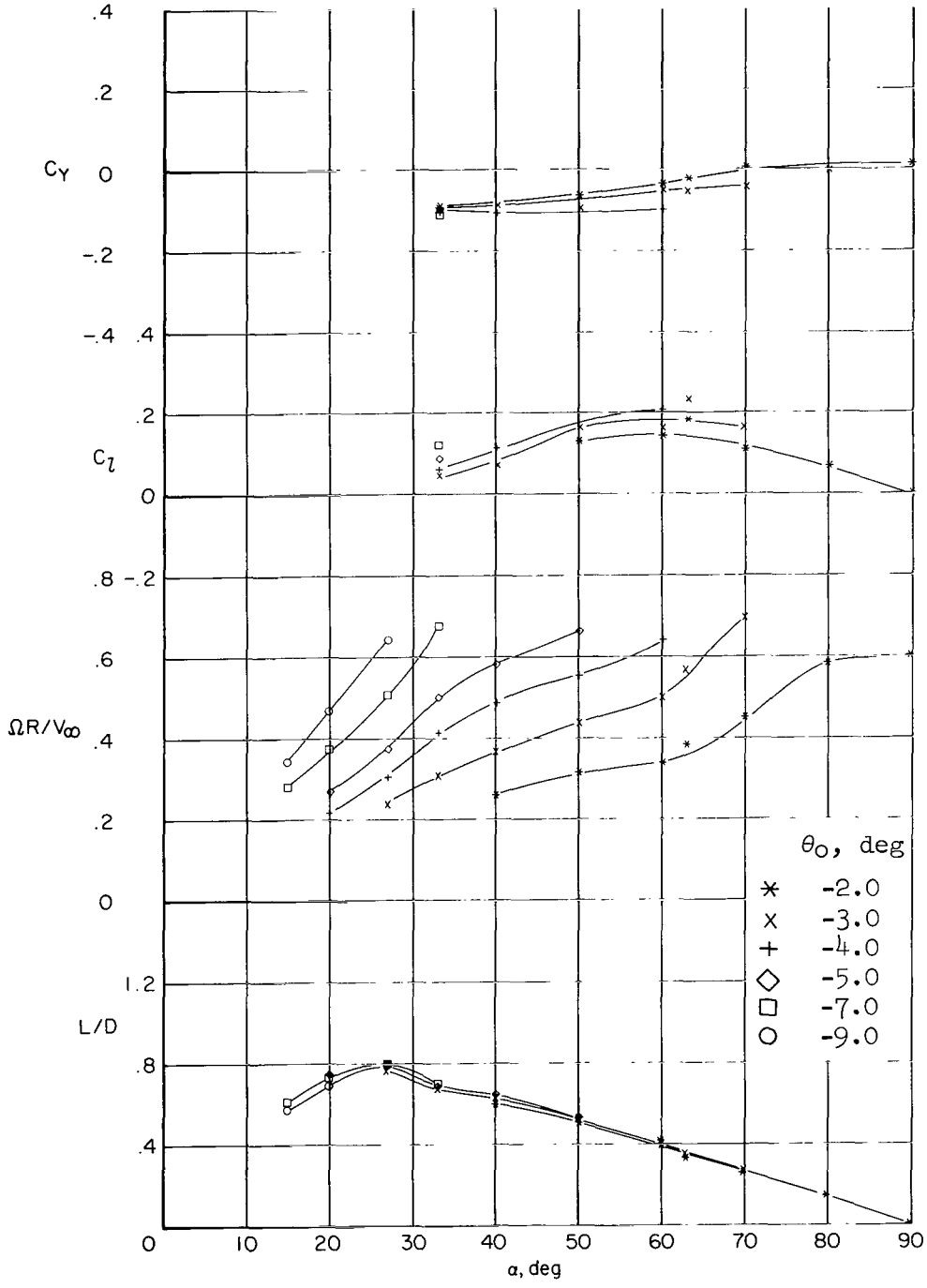

(a) M_∞ = 1.62 - Concluded.

Figure 12.- Continued.

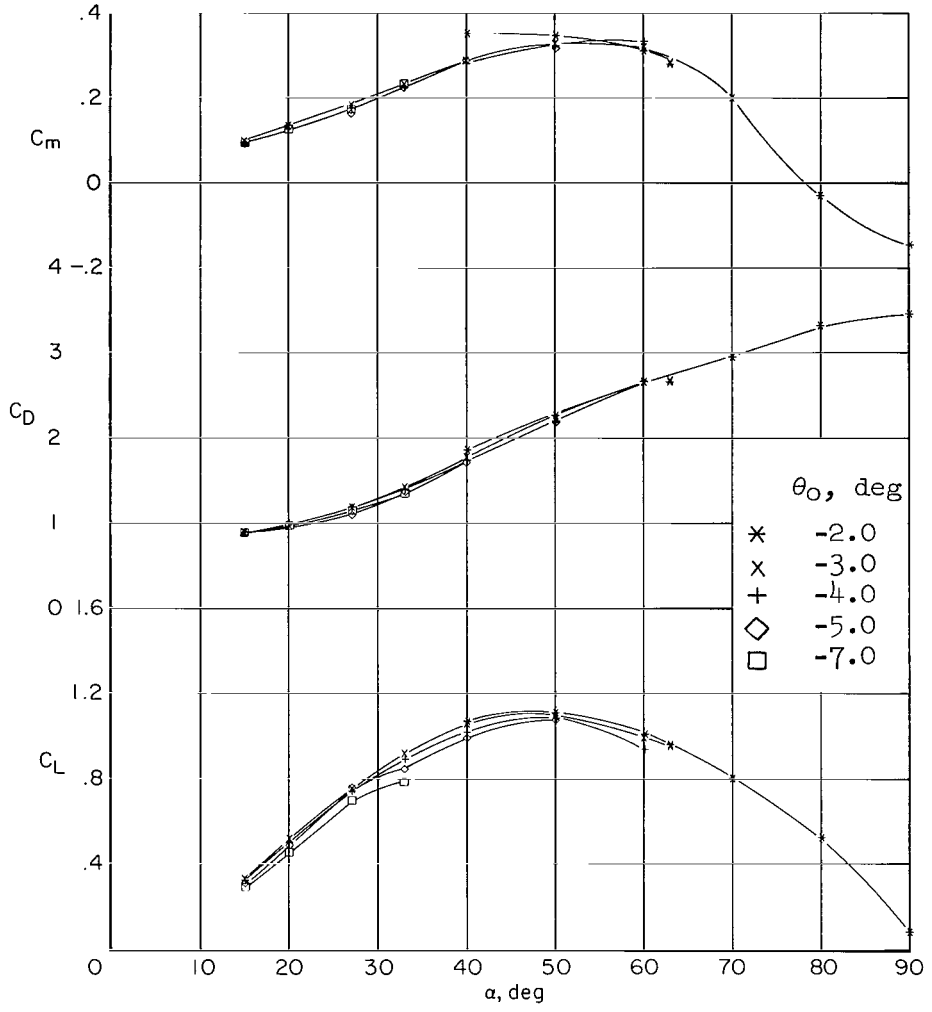

(b) $M_\infty = 3.54$

Figure 12.- Continued.

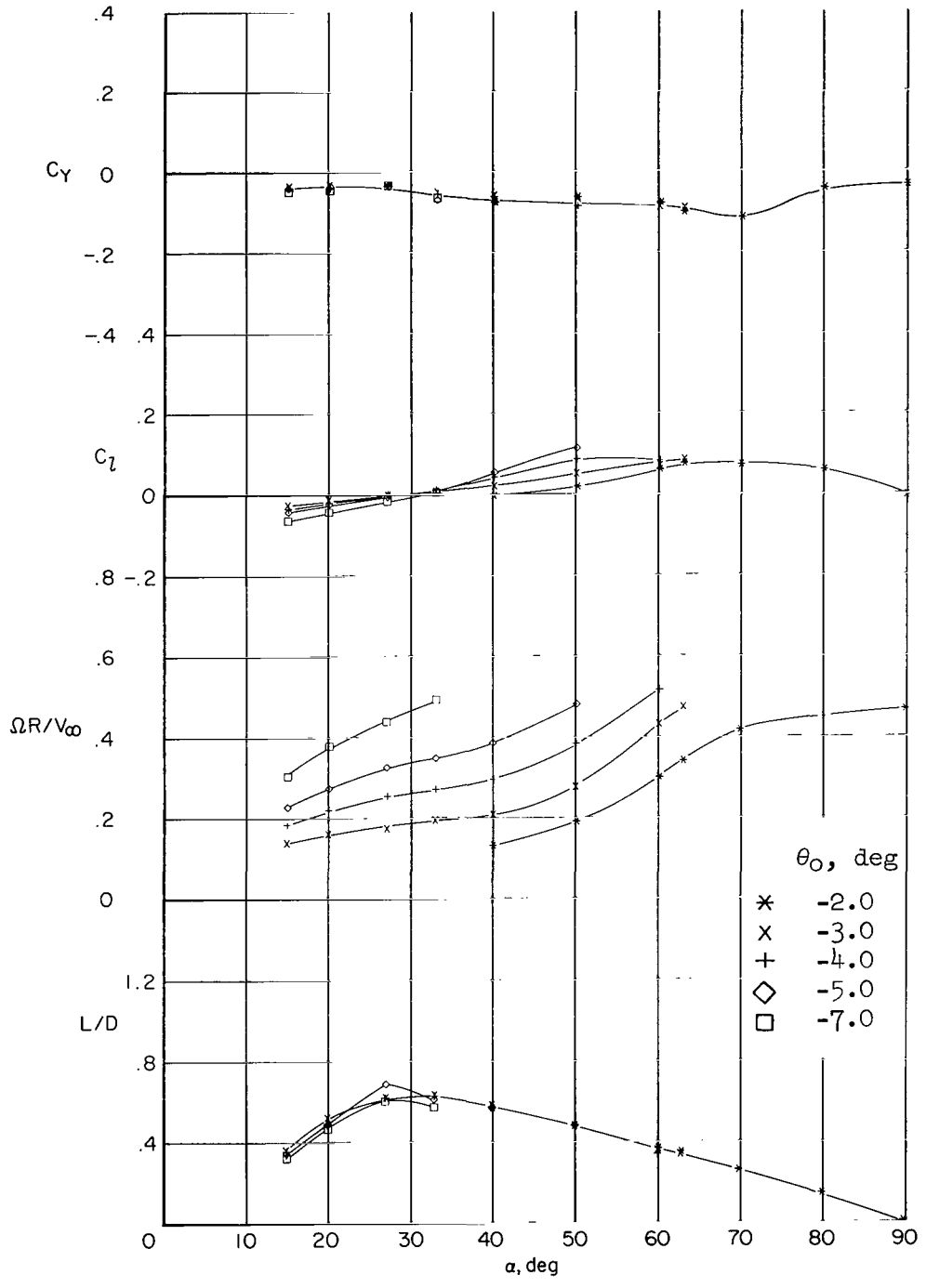

(b) $M_\infty = 3.54$ - Concluded.

Figure 12.- Concluded.

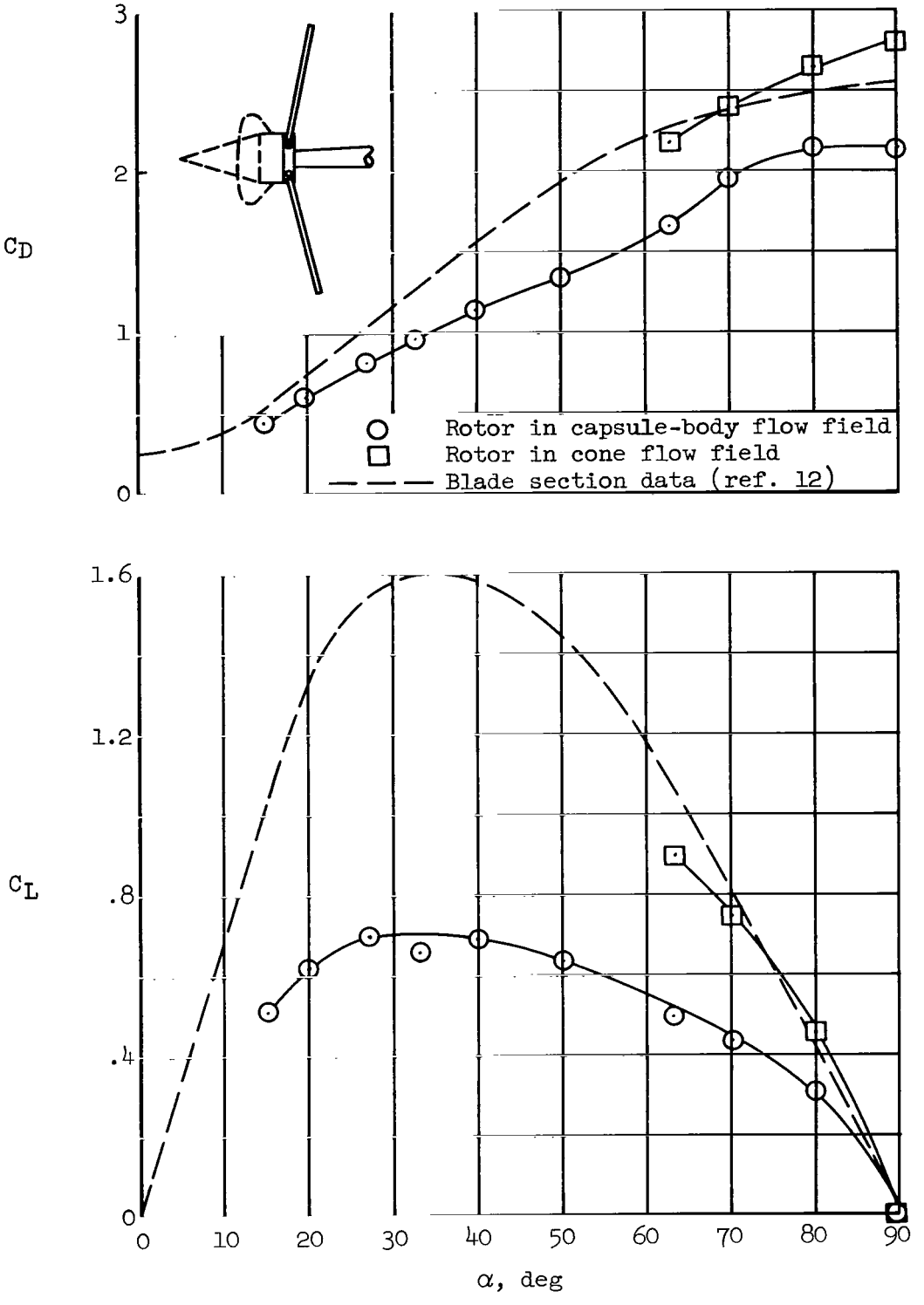

Figure 13.- Effect of forebody shape on rotor forces, elliptic-blade configuration; $M_\infty = 1.62$, $\theta_1 = 0^\circ$, $\theta_2 = 0^\circ$.

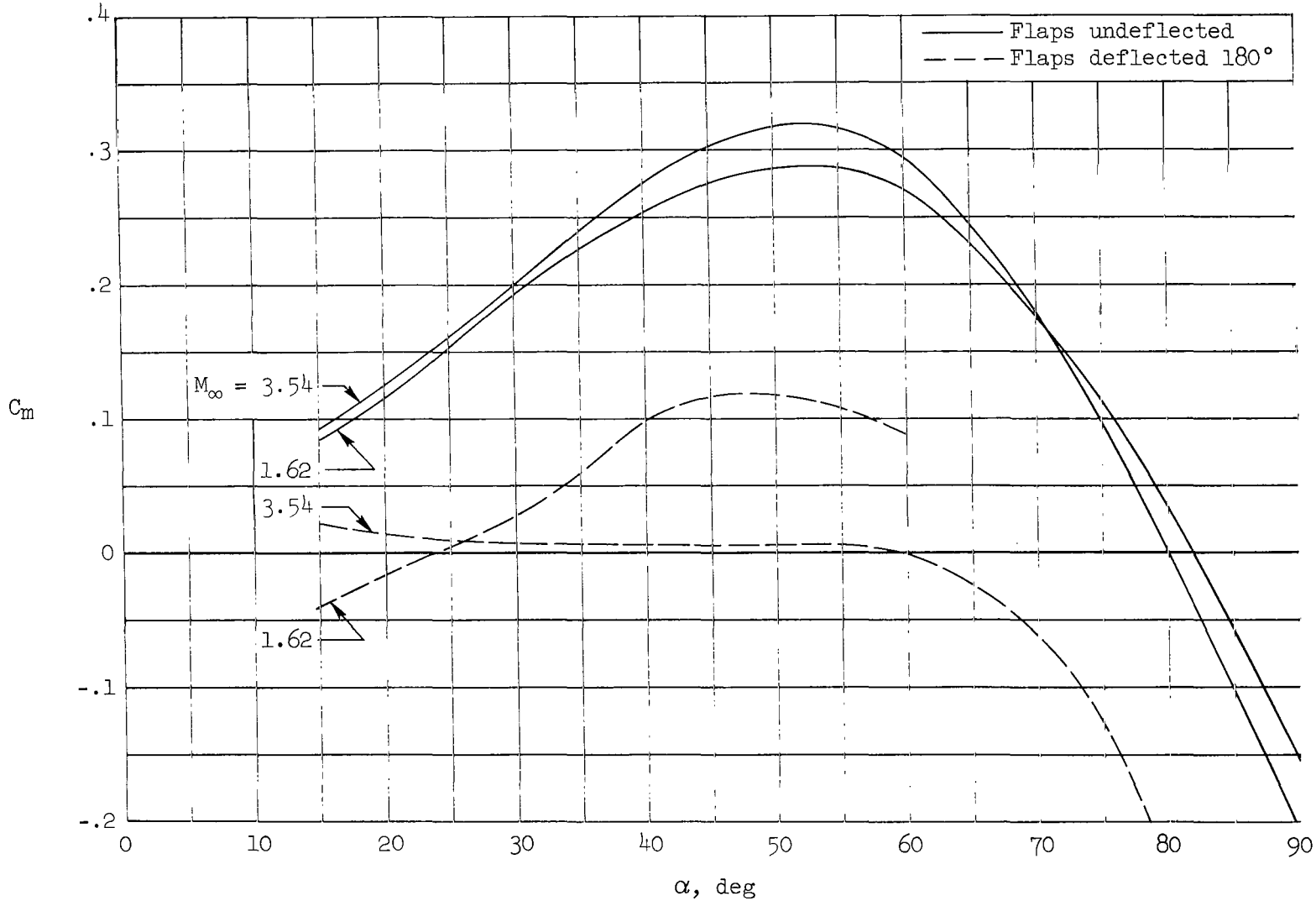

Figure 14.- Effect of pitch flaps on the longitudinal stability and trim characteristics of the elliptic-blade configuration.

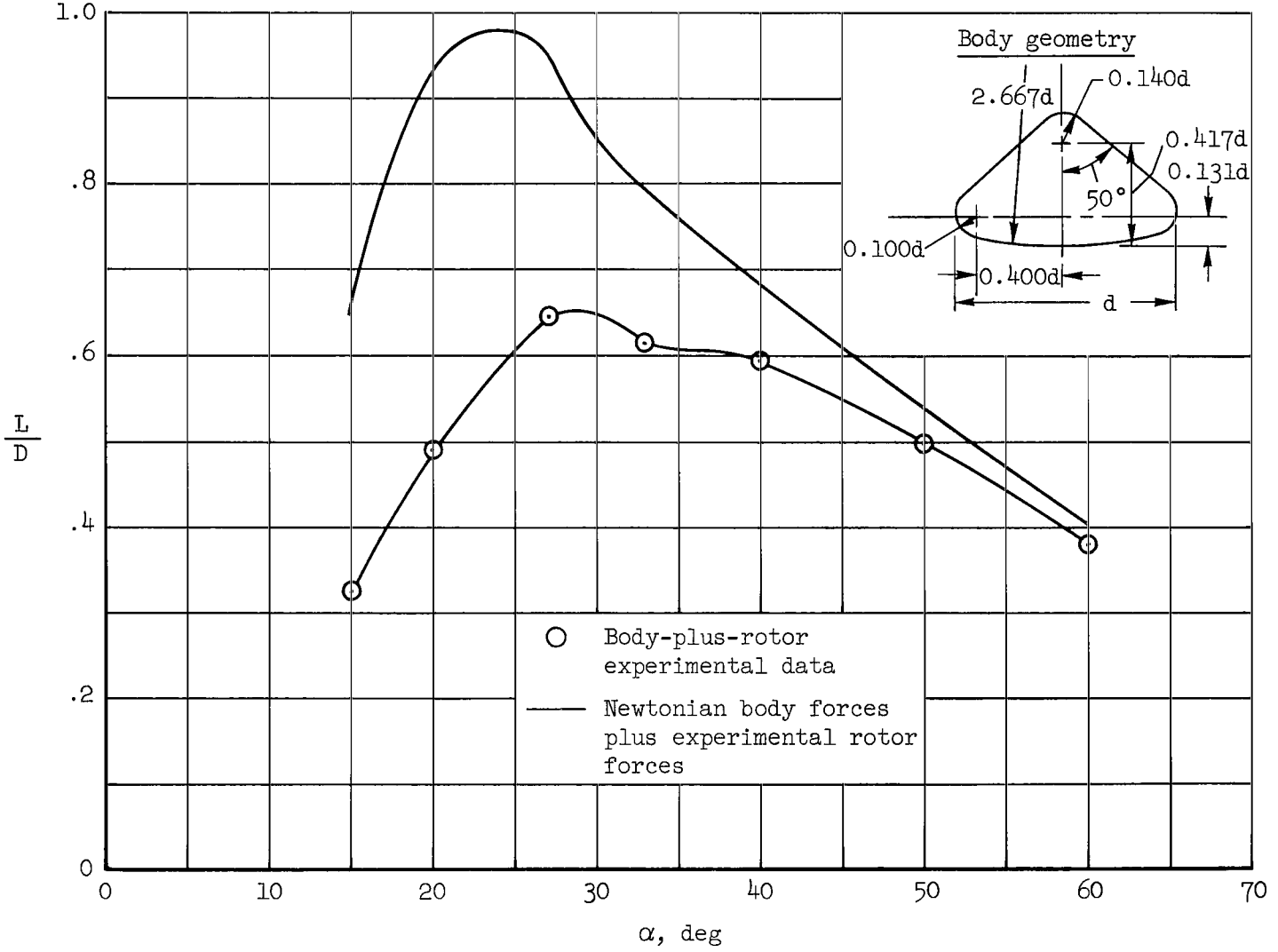

Figure 15.- Effect of removing drag due to oversized hub and blade grips on vehicle lift-drag ratio for elliptic-blade configuration; $M_\infty = 3.54$.

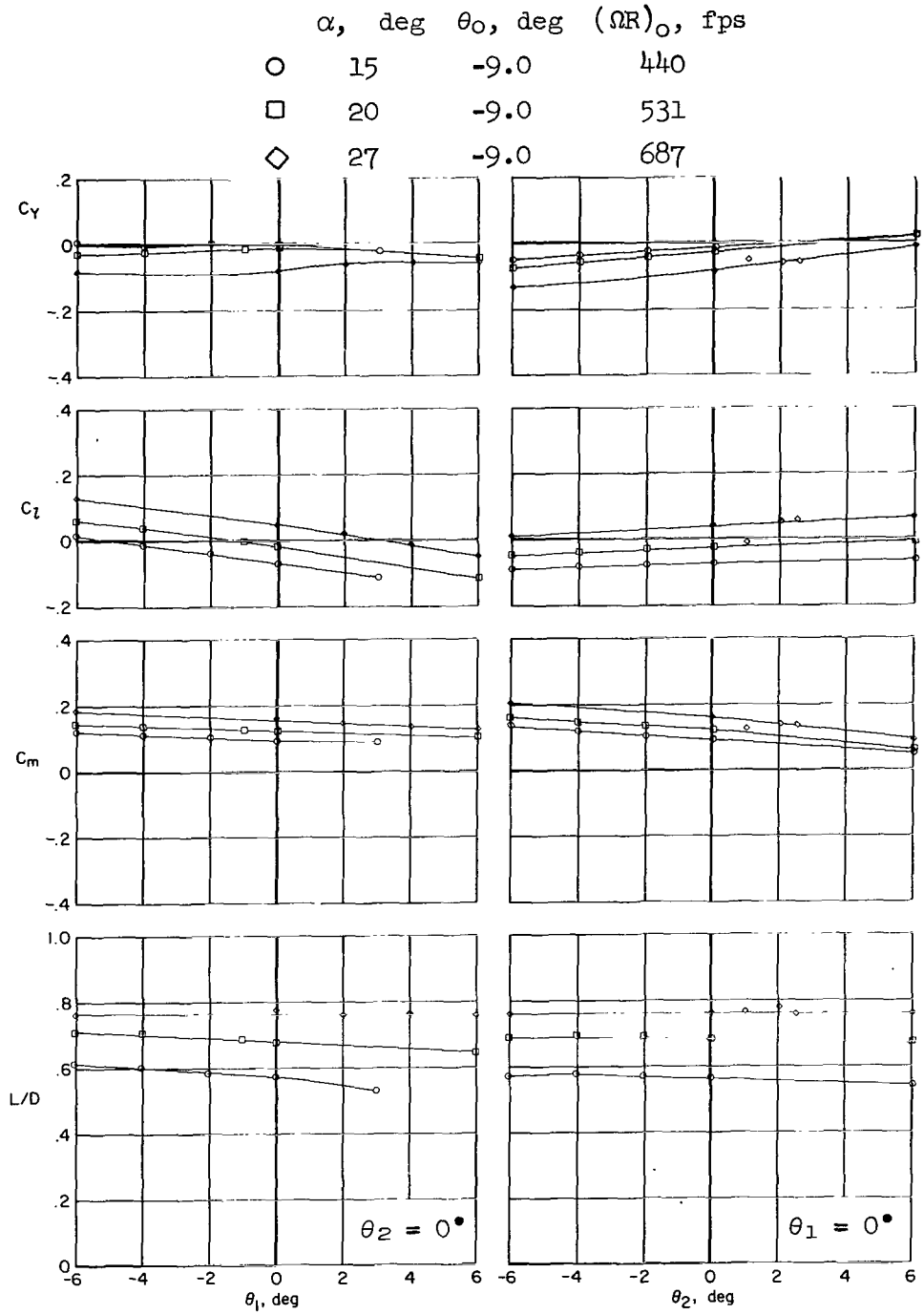

(a) $M_\infty = 1.62$; $\alpha = 15^\circ, 20^\circ, 27^\circ$

Figure 16.- Cyclic pitch control characteristics of the elliptic-blade configuration.

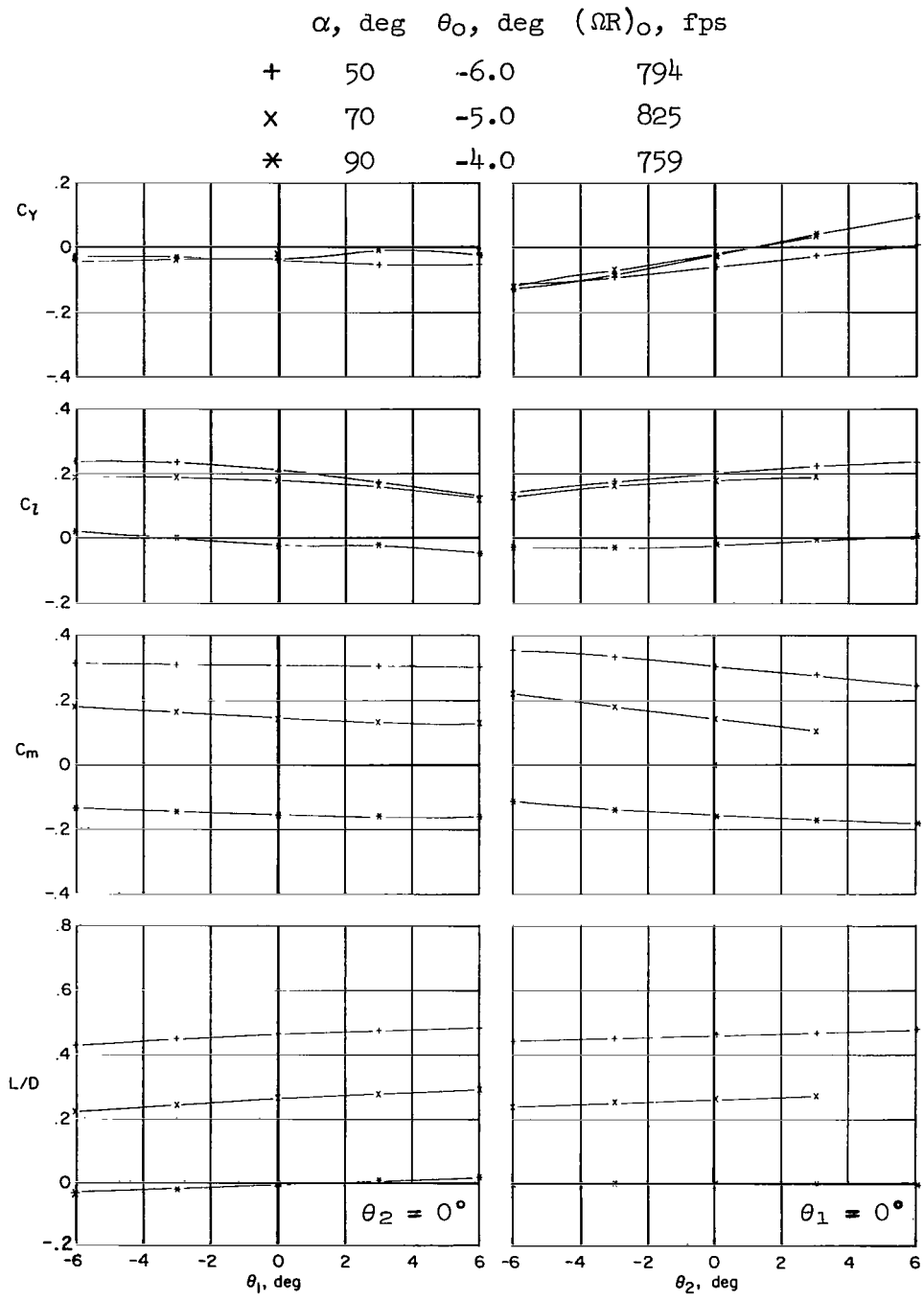

(b) $M_\infty = 1.62$; $\alpha = 50^\circ, 70^\circ, 90^\circ$

Figure 16.- Continued.

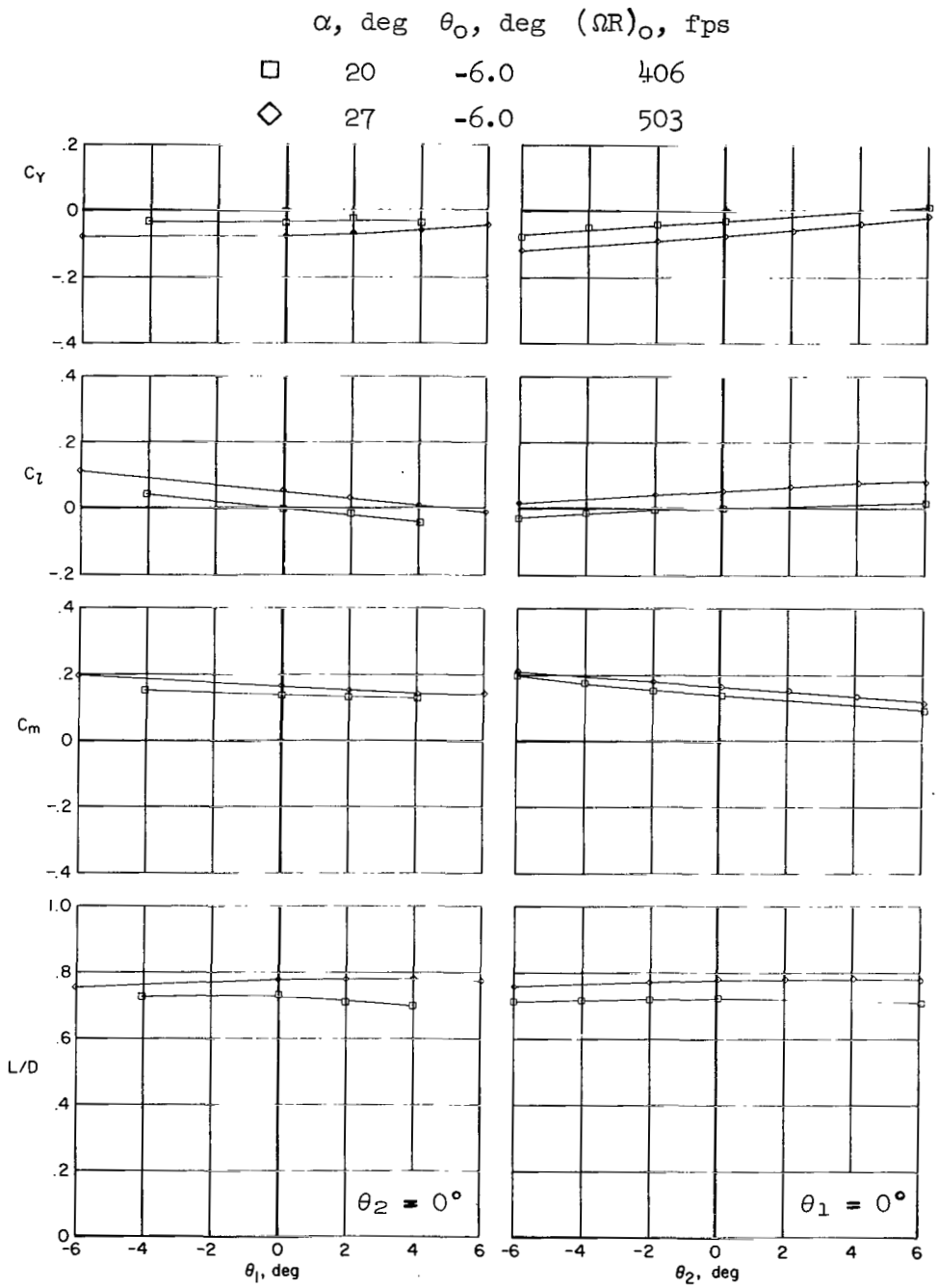

(c) $M_\infty = 1.62$; $\alpha = 20^\circ, 27^\circ$

Figure 16.- Continued.

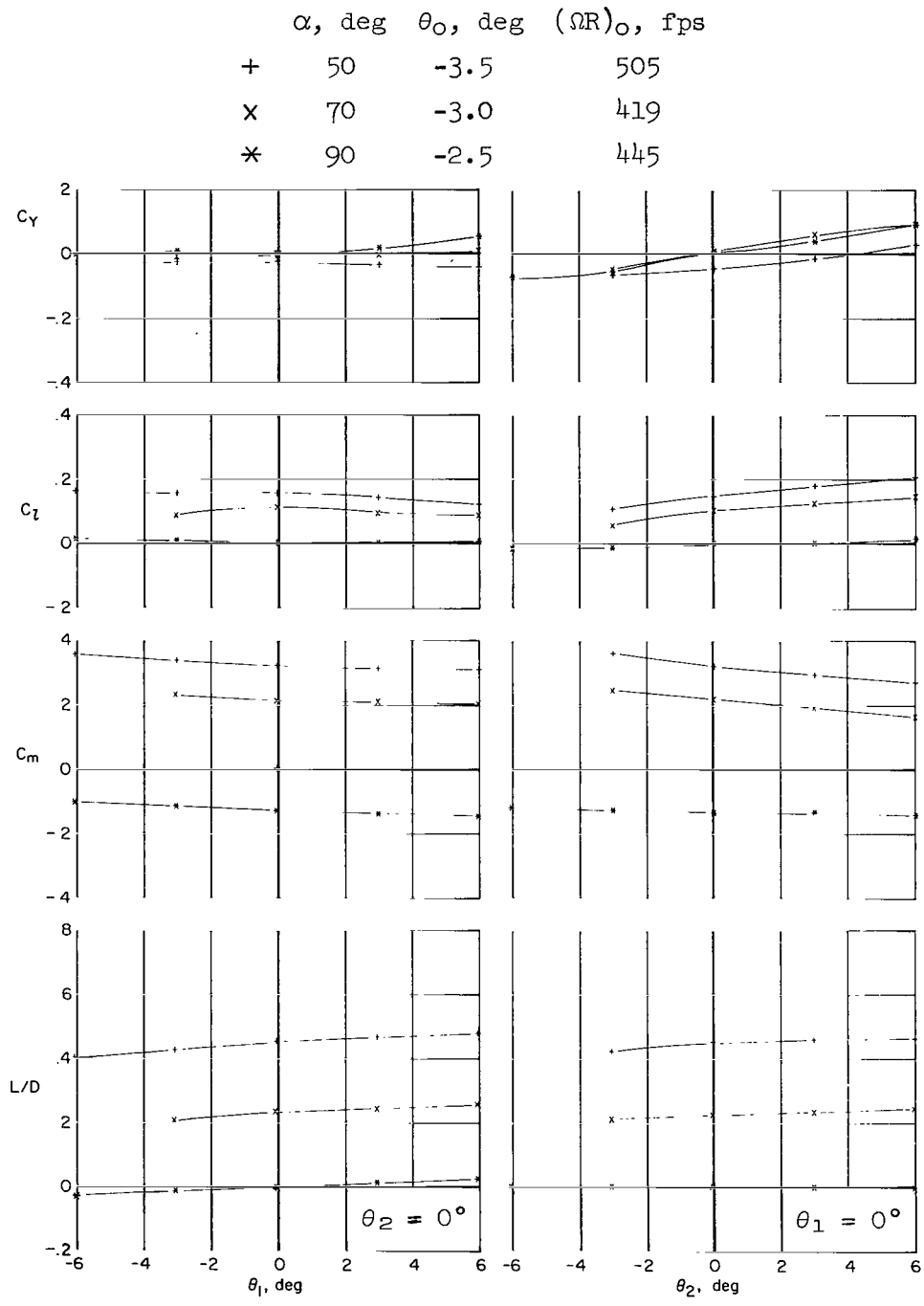

(d) $M_\infty = 1.62$; $\alpha = 50^\circ, 70^\circ, 90^\circ$

Figure 16.- Continued.

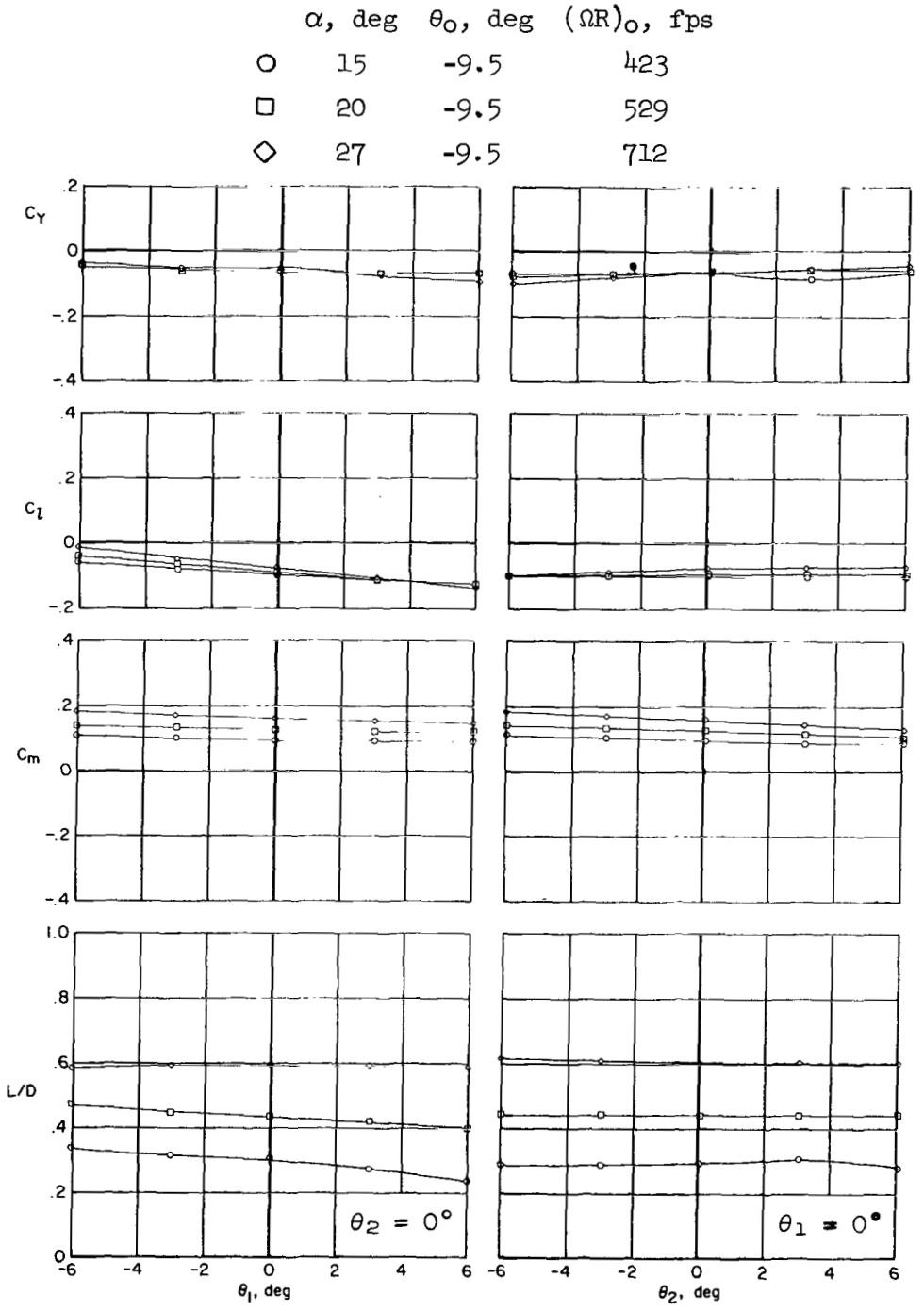

(e) $M_\infty = 3.54$; $\alpha = 15°, 20°, 27°$

Figure 16.- Continued.

	α, deg	θ_o, deg	$(\Omega R)_o$, fps
+	50	-5.5	776
x	70	-3.5	838
*	90	-3.0	885

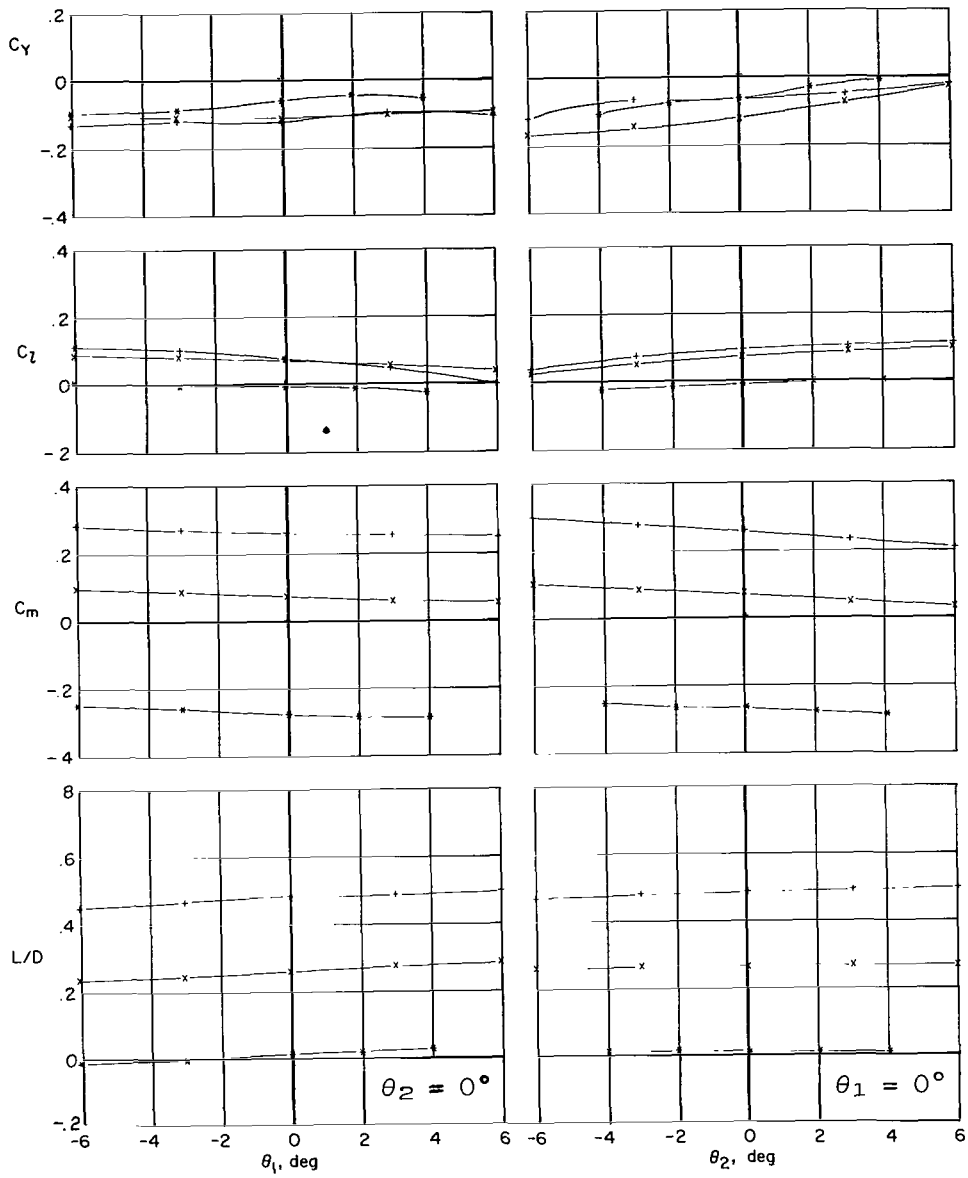

(f) $M_\infty = 3.54$; $\alpha = 50^\circ, 70^\circ, 90^\circ$

Figure 16.- Continued.

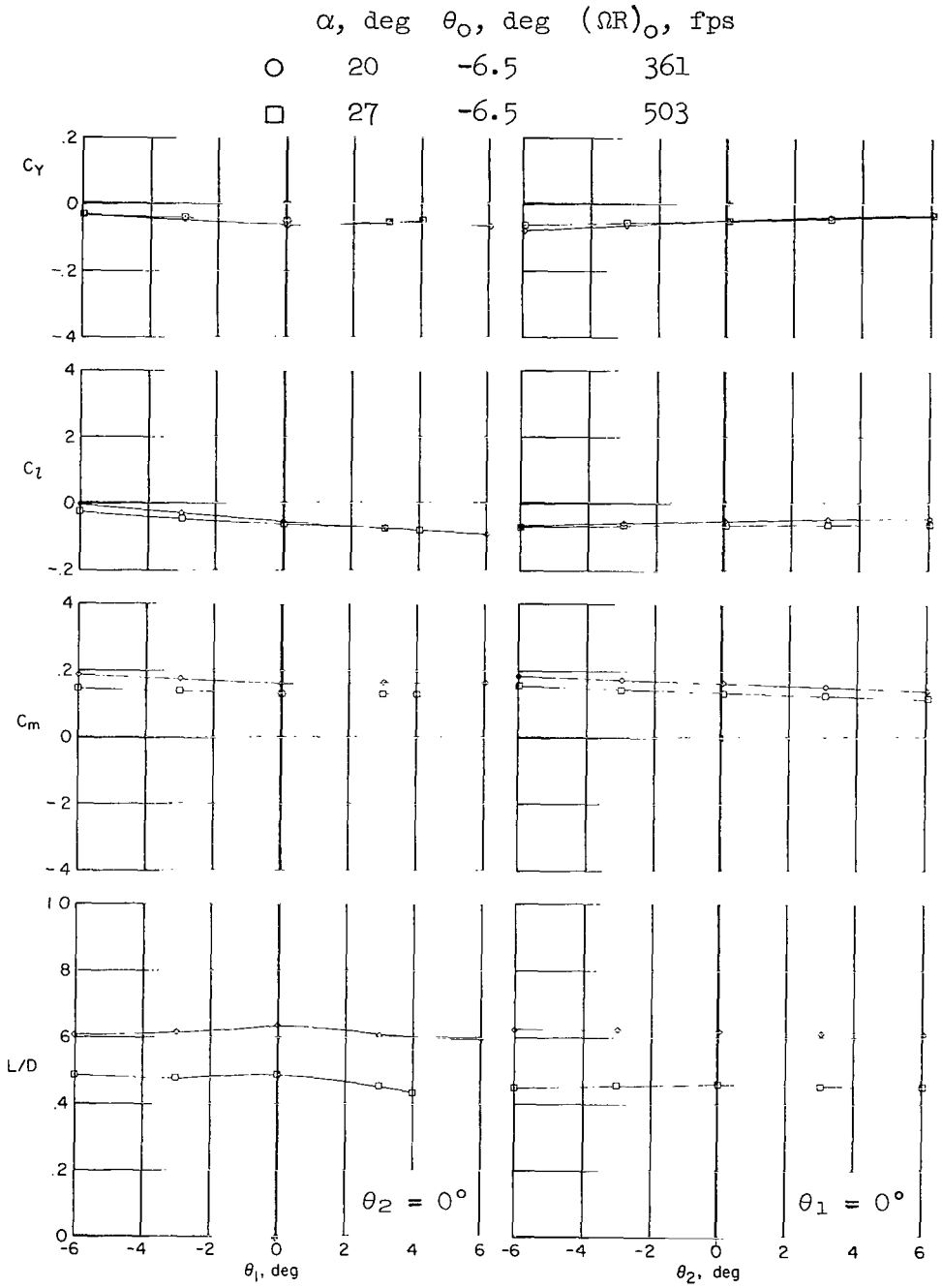

(g) $M_\infty = 3.54$; $\alpha = 20^\circ, 27^\circ$

Figure 16.- Continued.

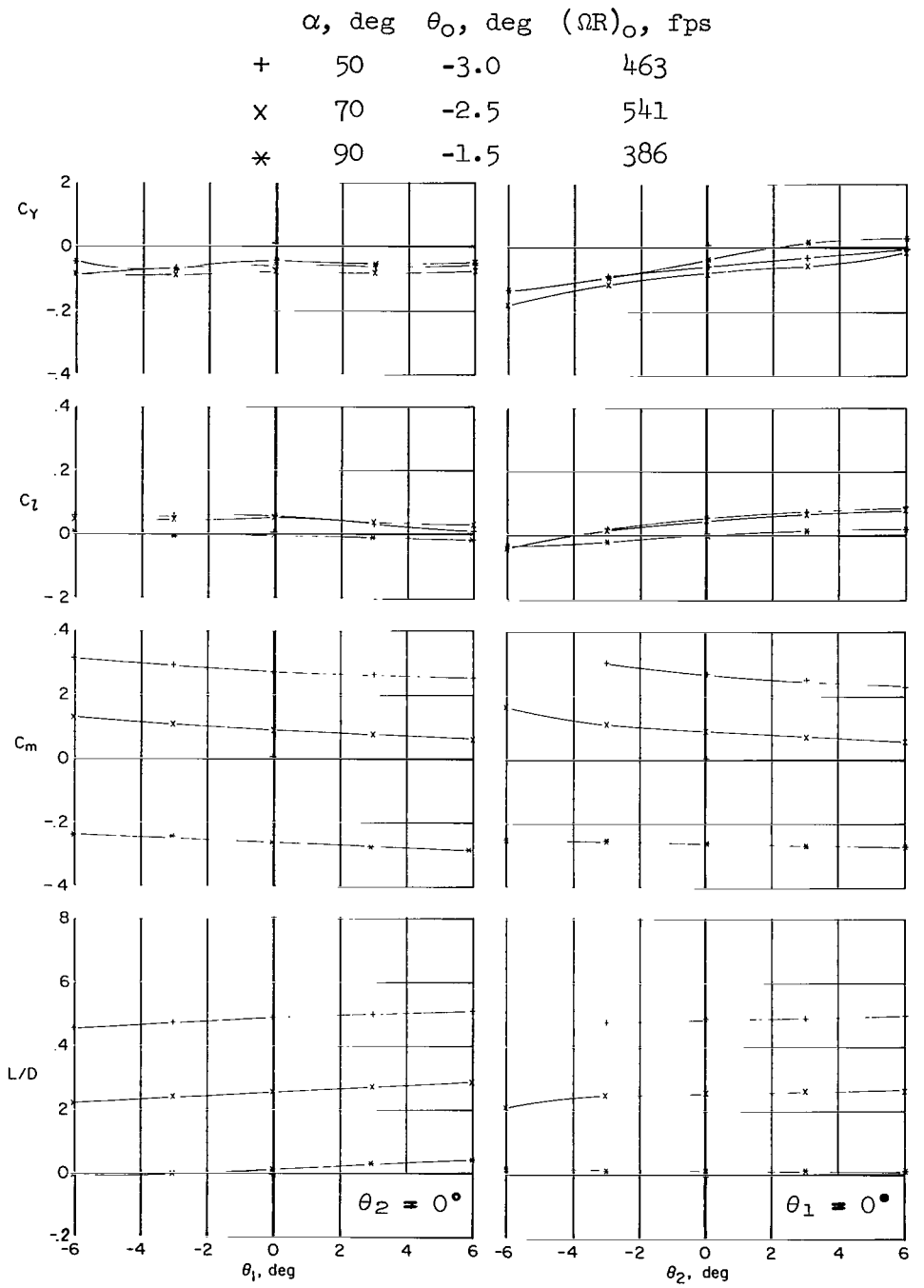

(h) $M_\infty = 3.54$; $\alpha = 50^\circ, 70^\circ, 90^\circ$

Figure 16.- Concluded.

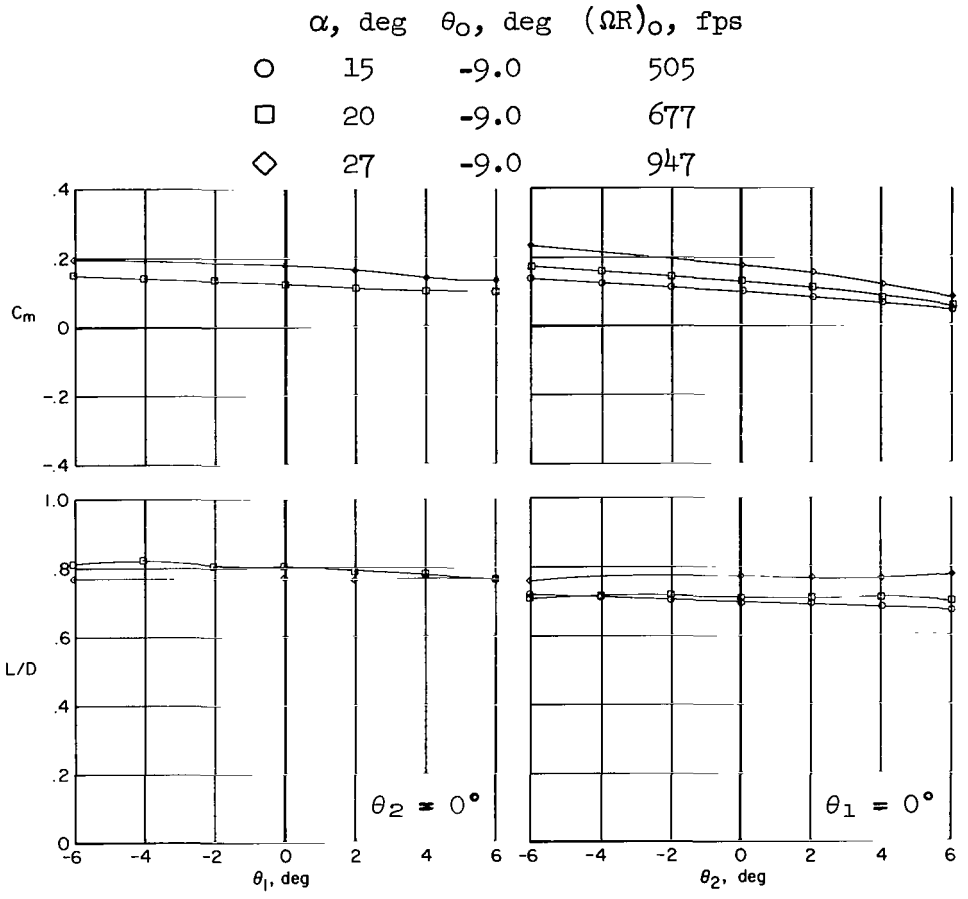

(a) $M_\infty = 1.62$; $\alpha = 15°, 20°, 27°$

Figure 17.- Cyclic pitch control characteristics of the double-wedge blade configuration.

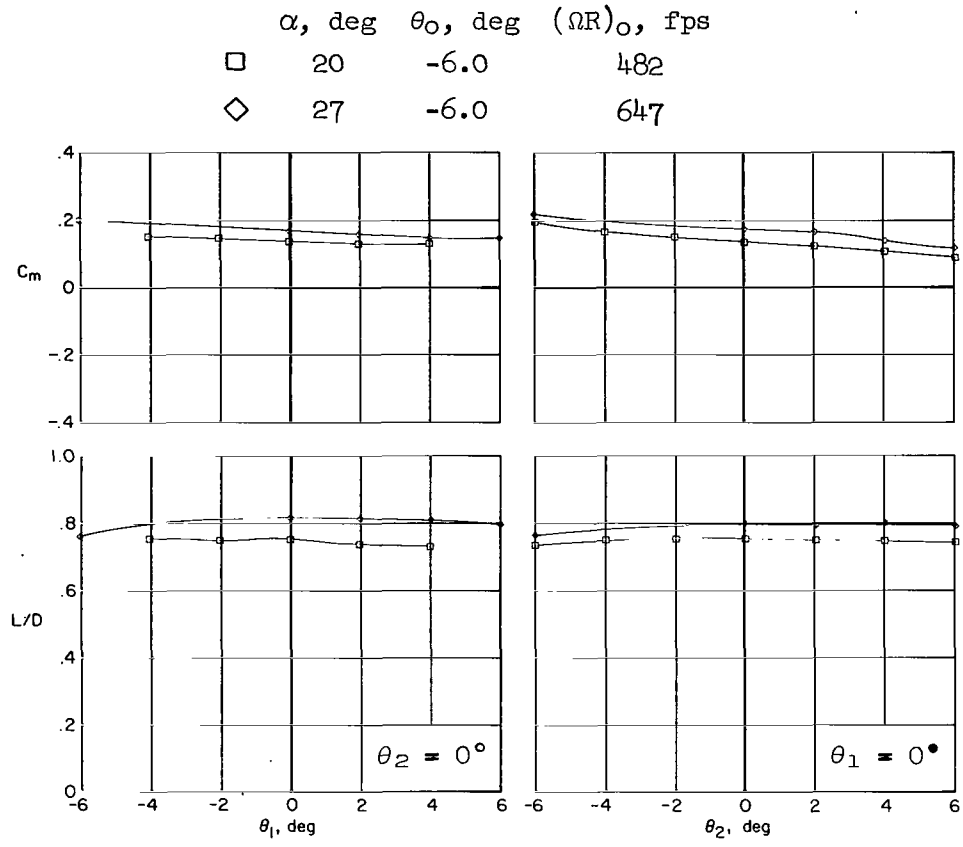

(b) $M_\infty = 1.62$; $\alpha = 20^\circ, 27^\circ$

Figure 17.- Continued.

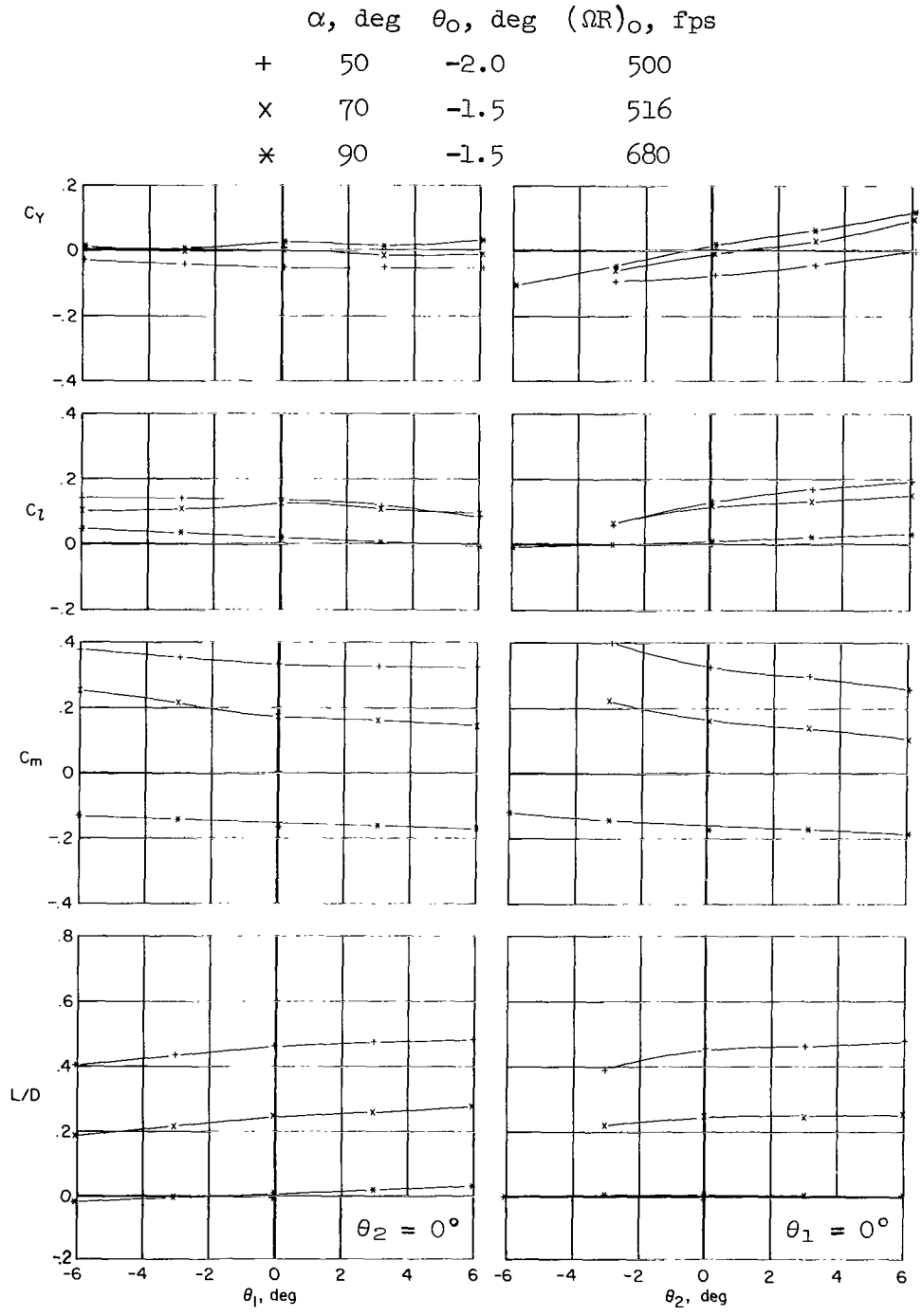

(c) $M_\infty = 1.62$; $\alpha = 50°, 70°, 90°$

Figure 17.- Continued.

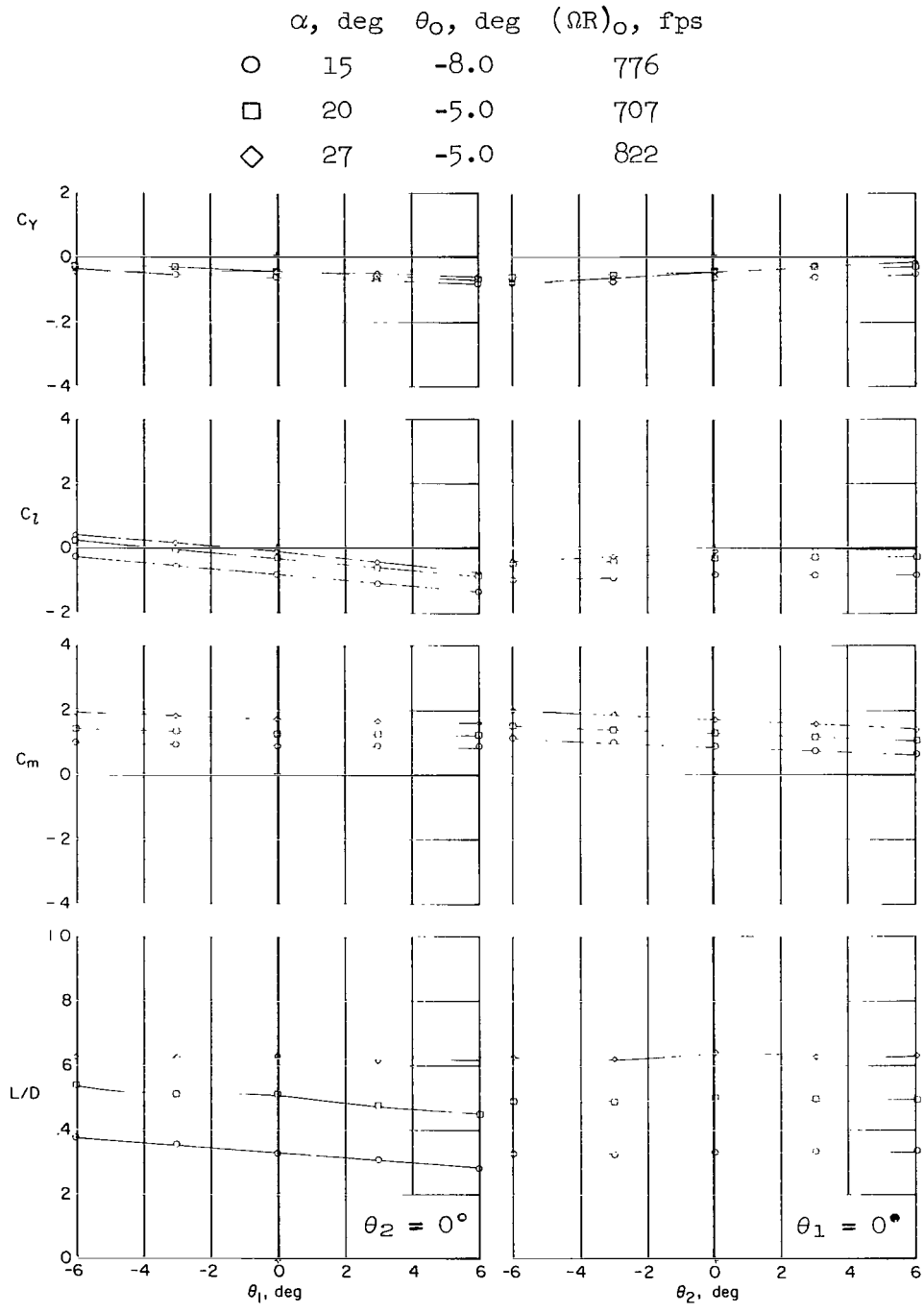

(d) $M_\infty = 3.54$; $\alpha = 15°, 20°, 27°$

Figure 17.- Continued.

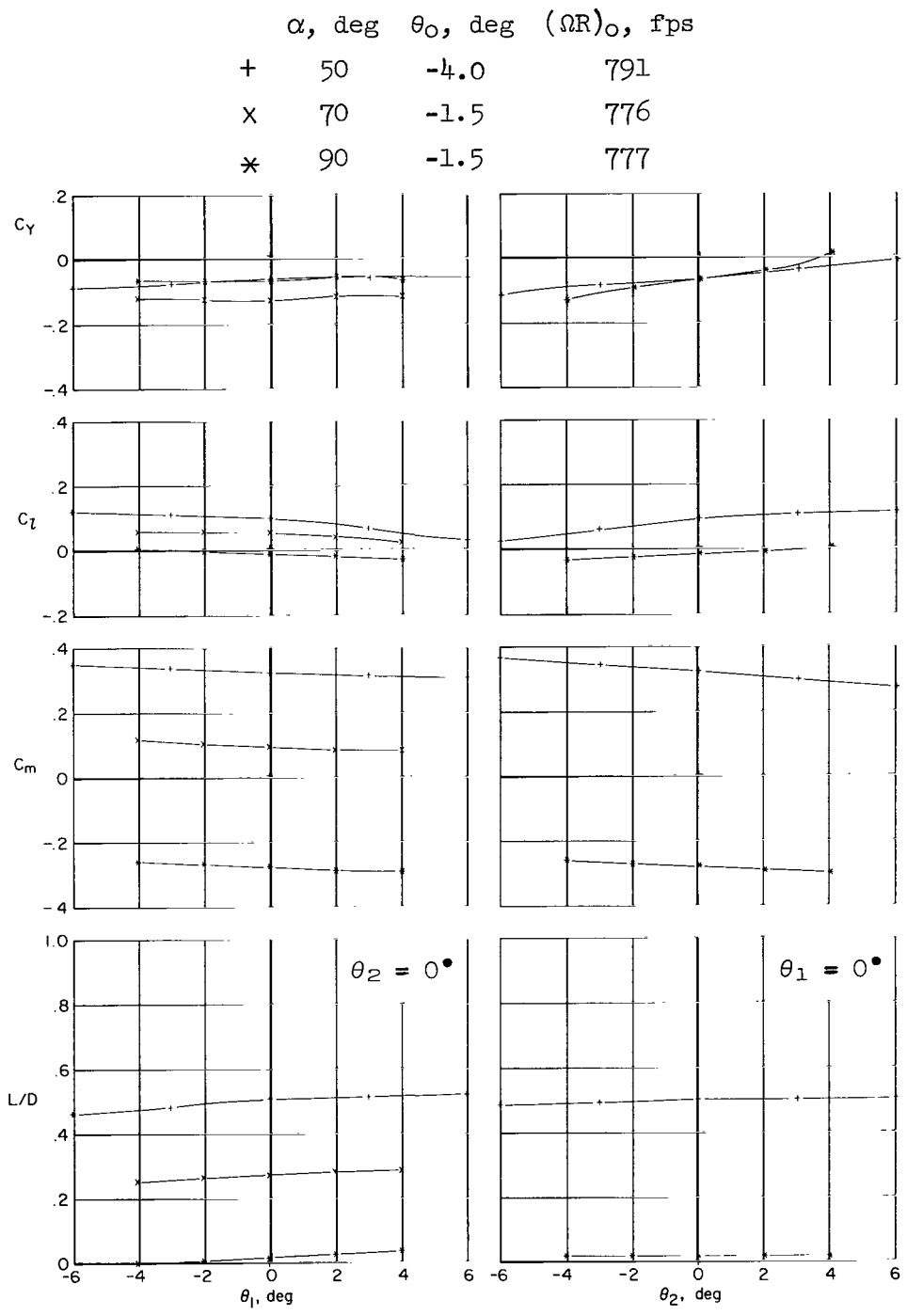

(e) $M_\infty = 3.54$; $\alpha = 50^\circ, 70^\circ, 90^\circ$

Figure 17.- Continued.

	α, deg	θ_o, deg	$(\Omega R)_o$, fps
+	50	-2.5	487
×	70	-1.0	510
*	90	-1.0	494

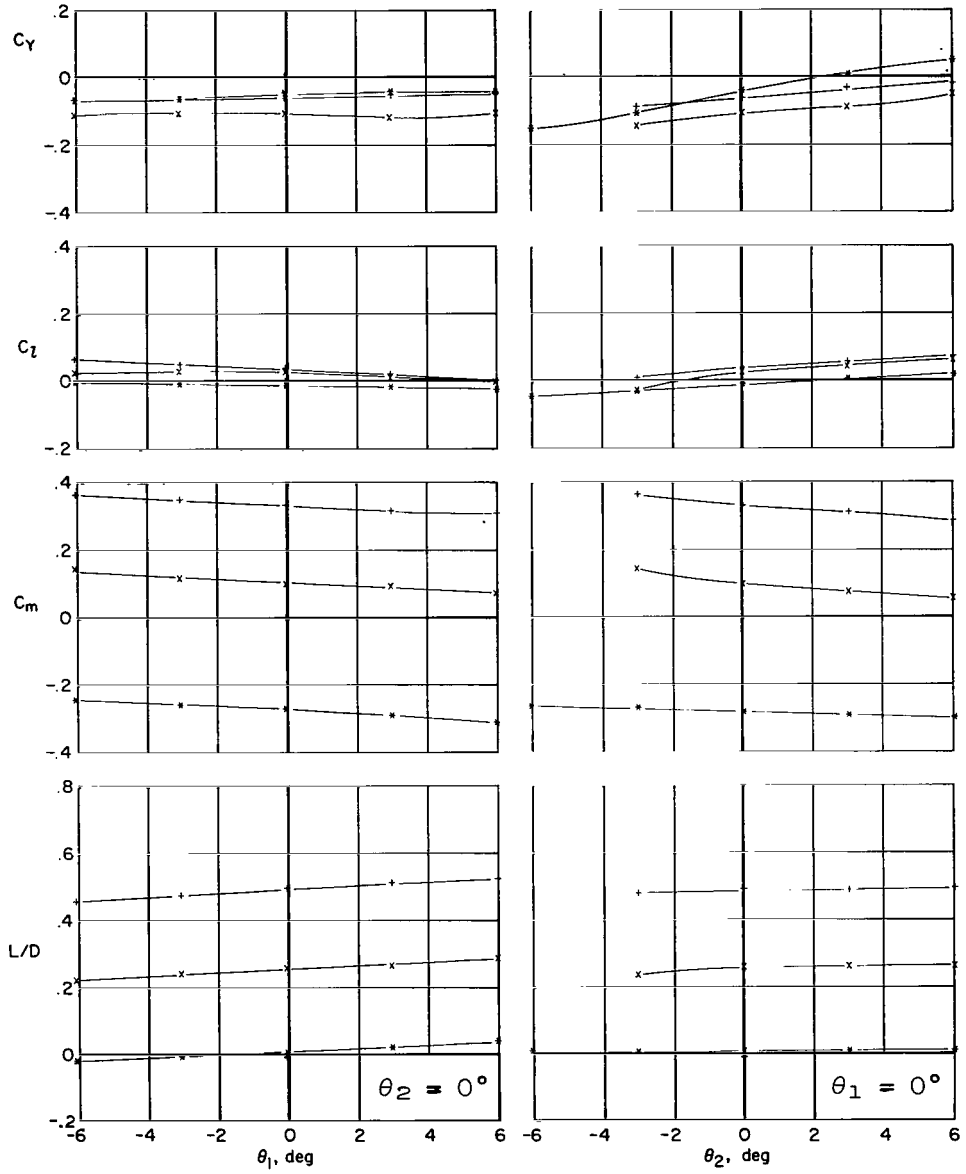

(f) $M_\infty = 3.54$; $\alpha = 50°, 70°, 90°$

Figure 17.- Concluded.

"The aeronautical and space activities of the United States shall be conducted so as to contribute . . . to the expansion of human knowledge of phenomena in the atmosphere and space. The Administration shall provide for the widest practicable and appropriate dissemination of information concerning its activities and the results thereof."

—NATIONAL AERONAUTICS AND SPACE ACT OF 1958

NASA SCIENTIFIC AND TECHNICAL PUBLICATIONS

TECHNICAL REPORTS: Scientific and technical information considered important, complete, and a lasting contribution to existing knowledge.

TECHNICAL NOTES: Information less broad in scope but nevertheless of importance as a contribution to existing knowledge.

TECHNICAL MEMORANDUMS: Information receiving limited distribution because of preliminary data, security classification, or other reasons.

CONTRACTOR REPORTS: Scientific and technical information generated under a NASA contract or grant and considered an important contribution to existing knowledge.

TECHNICAL TRANSLATIONS: Information published in a foreign language considered to merit NASA distribution in English.

SPECIAL PUBLICATIONS: Information derived from or of value to NASA activities. Publications include conference proceedings, monographs, data compilations, handbooks, sourcebooks, and special bibliographies.

TECHNOLOGY UTILIZATION PUBLICATIONS: Information on technology used by NASA that may be of particular interest in commercial and other non-aerospace applications. Publications include Tech Briefs, Technology Utilization Reports and Technology Surveys.

Details on the availability of these publications may be obtained from:

SCIENTIFIC AND TECHNICAL INFORMATION OFFICE

NATIONAL AERONAUTICS AND SPACE ADMINISTRATION

Washington, D.C. 20546